CONF-8310198--3

MECHANICAL PROPERTIES OF TYPES 304 AND 316 STAINLESS STEEL AFTER LONG-TERM AGING AND EXPOSURE*

J. A. Horak and V. K. Sikka
Metals and Ceramics Division, Oak Ridge National Laboratory,
Oak Ridge, Tennessee 37831, USA

and

D. T. Raske
Argonne National Laboratory,
Argonne, Illinois 60439

CONF-8310198--3

DE84 003325

ABSTRACT

Because designs for Liquid Metal Fast Breeder Reactor (LMFBR) power plants include plant lifetimes to 40 years, an understanding of the mechanical behavior of the structural alloys used is required for times of ~2 to 2.5 × 10^5 h. Most of the alloys used for LMFBR out-of-core structures and components are in a metastable state at the beginning of plant lifetime and evolve to a more stable state and, therefore, microstructure during plant operation. We reviewed mechanical properties and microstructures after prolonged elevated-temperature exposure of types 304 and 316 stainless steel, two alloys used extensively in fast breeder systems. Aging alters properties; in particular, it decreases toughness and tensile ductility, but the properties are still adequate for service. Because stable microstructures have been reached in long-term exposures achieved so far, properties can be expected to remain adequate for service life exposures.

INTRODUCTION

Liquid Metal Fast Breeder Reactor (LMFBR) power plants are designed for lifetimes of up to 40 years. For these plants to operate safely and reliably, which also translates to economically, for their full lifetimes requires that the major components of the plant must also perform satisfactorily for similar times, usually for the full plant lifetime. If the LMFBR is to fulfill its potential role in providing energy self-sufficiency, major structures and components must also perform reliably for long operating times, preferably for the design life of the plant. The energy production and revenue lost because of the required replacement of any structures or components, combined with the replacement cost of the structure or component and the expense of purchased power during such an

*Research sponsored by the Office of Breeder Technology Projects, Office of Nuclear Energy, U.S. Department of Energy, under contract W-7405-eng-26 with Union Carbide Corporation.

unscheduled outage, would seriously affect the cost of electricity and fuel produced by the breeder. If frequent shutdowns are required for repair or replacement of major structures and components in near-term LMFBRs, the breeder would most probably not have the opportunity to penetrate the utility marketplace or make a significant contribution to energy self-sufficiency.

To ensure that the plant meets its design objectives requires the capability to predict materials behavior for times of about 2×10^5 h, which is the full 40-year design lifetime at a capacity factor of 70%. To predict materials behavior for anticipated plant lifetimes requires both a quantitative understanding of the microstructural changes that can occur in these structural alloys during exposure to LMFBR operating environments and proven correlations between these microstructures and the mechanical properties of these alloys. Such understanding and correlations are also required to interpolate materials behavior to systems conditions that are intermediate to those used in laboratory tests to develop the mechanical properties design data, to predict the response of components and structures to off-normal operating conditions, and to provide the information necessary to scale up from laboratory test conditions and specimen sizes to full-size reactor components and structures.

Structural alloys are in a metastable thermodynamic state at the beginning of plant lifetime. During prolonged exposure to the temperatures and stresses of LMFBR operation, these alloys evolve to more stable thermodynamic states and microstructures. As the microstructures change, the mechanical properties also change. Knowledge of the relationships between mechanical properties and the microstructures that evolve under plant operating conditions enables the needed extrapolations and interpolations from test data to operating lifetimes.

Weiss and Stickler reported the thermodynamic and microstructural changes that occur in type 316 stainless steel when the single-phase solid solution austenite is exposed to elevated temperatures for prolonged times.[1] They developed the time-temperature precipitation diagram for type 316 stainless steel, which describes the formation of $M_{23}C_6$, eta, chi, and sigma phases as a function of time and temperature. They have also reported the changes in the low-temperature Charpy impact strength that are associated with the precipitation of these phases. Formation of eta and chi phases results in a large decrease in the low-temperature (below room temperature) Charpy impact strength. The Charpy impact strength reaches the lowest values observed when sigma phase is observed in the microstructure. This information will be used later in this paper in the discussion of long-term service exposure or aging of type 316 stainless steel and its weldments with type 16-8-2 filler metal and in the discussion of stainless steel castings.

Types 304 and 316 stainless steel and their associated weld metals have been the major structural materials for all fast neutron test facilities and experimental fast reactors built or planned to date in the United States, including the Clinch River Breeder Reactor (Fig. 1) (ref. 2). Because of the excellent performance of these alloys in those facilities and their extensive use in current and future U.S. LMFBR designs, this paper treats these two alloys and, to a considerably lesser extent, weld

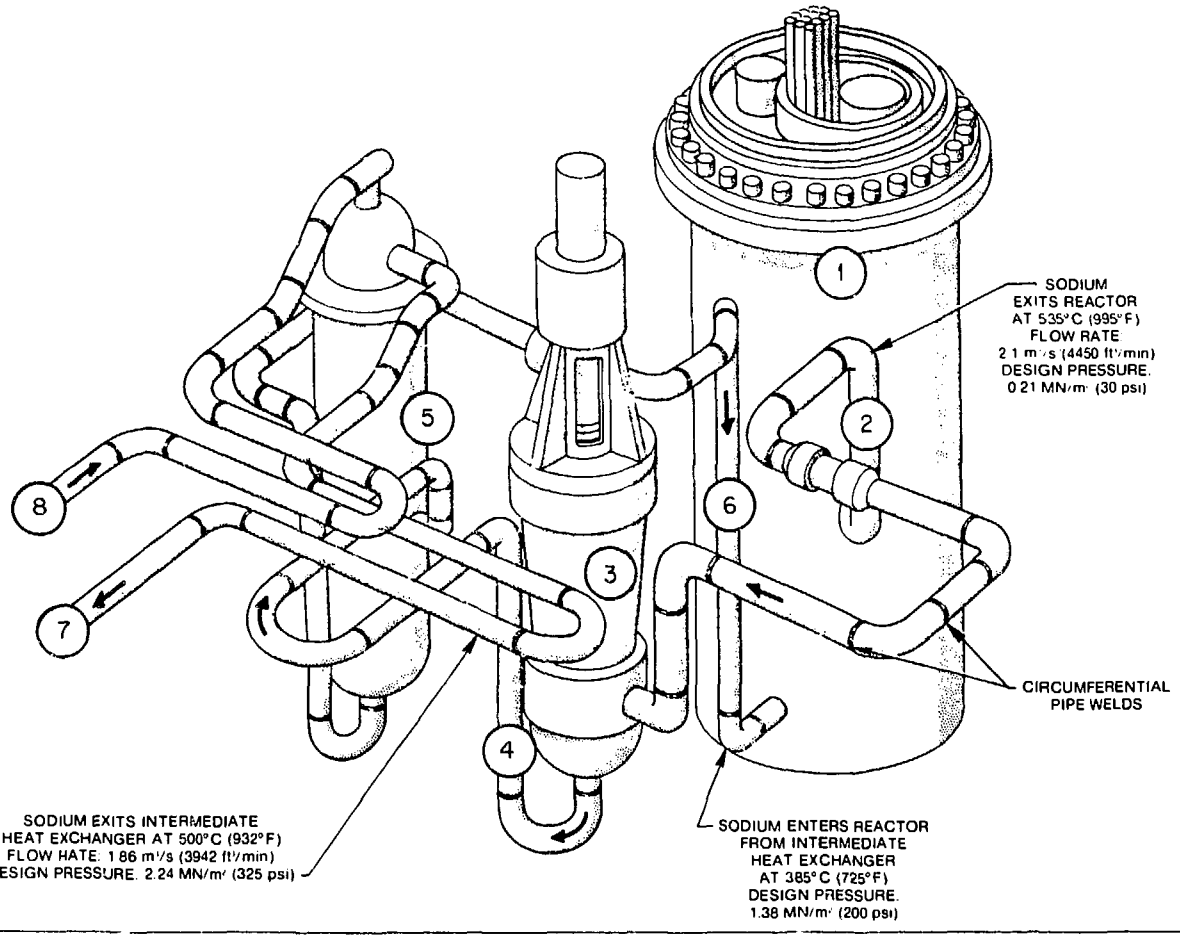

Fig. 1. Uses of types 304 and 316 stainless steel and their weldments for Clinch River Breeder Reactor out-of-core structures and components.

filler metals used with them. This paper presents information on the mechanical properties of these alloys after long-term (10^4–10^5 h) elevated-temperature (>0.40T_m) (T_m = absolute melting point) exposure (i.e., aging), after creep, and after fatigue deformation and on microstructural evolution during long-term testing and aging. An attempt is made to relate the measured changes in properties to the observed changes in microstructure and to provide a consistent coherent explanation for the properties-microstructure relationship. Included is the use of the existing property and microstructure data bases for applications to long-term plant operating conditions.

EXPERIMENTAL DATA AND DISCUSSION

WROUGHT MATERIALS

Tensile Properties

The effects of laboratory aging or service exposure to times up to 5.1×10^4 h at temperatures up to 649°C (1200°F) on the microstructure and tensile properties of mill-annealed type 316 stainless steel are shown in Fig. 2 (ref. 3). In the unaged condition the microstructure shows only high-angle grain boundaries. After six months (4×10^3 h) at 649°C (1200°F) large carbide precipitate particles are present on these boundaries. After six years (5.1×10^4 h) at this temperature carbide precipitation has occurred within the grains as well as at the grain boundaries. Six years of exposure at this temperature (which is 0.53T_m for this alloy) has resulted in C, Cr, Ni, and Mo that originally were in solid solution being precipitated from the matrix into the large particles shown in Fig. 2. The strength properties at elevated temperature are still within the scatter band of the data for the strength properties of unaged material.

However, the total elongation of material removed from service in a fossil power plant after six years lies below that for unaged material for all test temperatures. Because the solid-solution-strengthening elements have been precipitated from the matrix, the matrix within the grains should be very ductile; hence, these lower ductilities must be associated with grain boundaries and the phases precipitated on these boundaries. In addition, reannealing for 0.5 h at 1065°C (1950°F) after this exposure history provides little recovery of the ductility, but the strength properties after reannealing are unchanged or exhibit further decrease. The decreased ductility after thermal exposure indicates that the aged material would possess less toughness at the relatively high strain rates of about 7×10^{-4}/s and less resistance to fracture (leak before break) than does the unaged material. Only the material exposed to the fossil plant operating environment exhibits the lower ductility. This environment may have a detrimental effect on the ductility at 649°C (1200°F) if significant oxidation and surface deterioration should occur in six years. Even for this worst condition the minimum total elongation exceeds 20%. This should be adequate to ensure the integrity of out-of-core structures and components for LMFBRs.

Additional information on the effects of longer term aging on the tensile properties of type 316 stainless steel is contained in Figs. 3 and 4. The data in Fig. 2 are for only 4 aging times, but those in Figs. 3

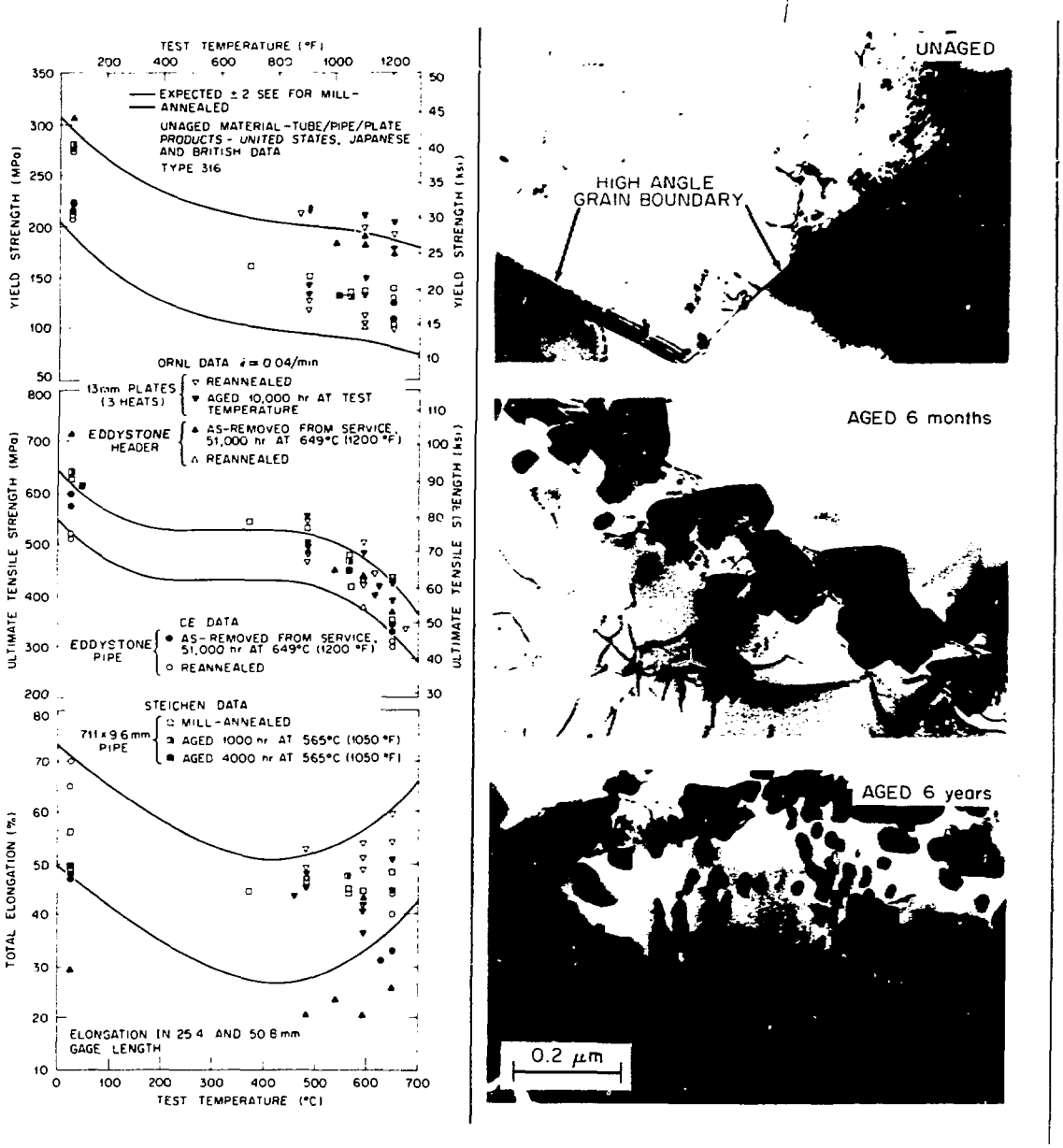

Fig. 2. Tensile properties and microstructures of type 316 stainless steel annealed and after aging for up to 51,000 h.

DISCLAIMER

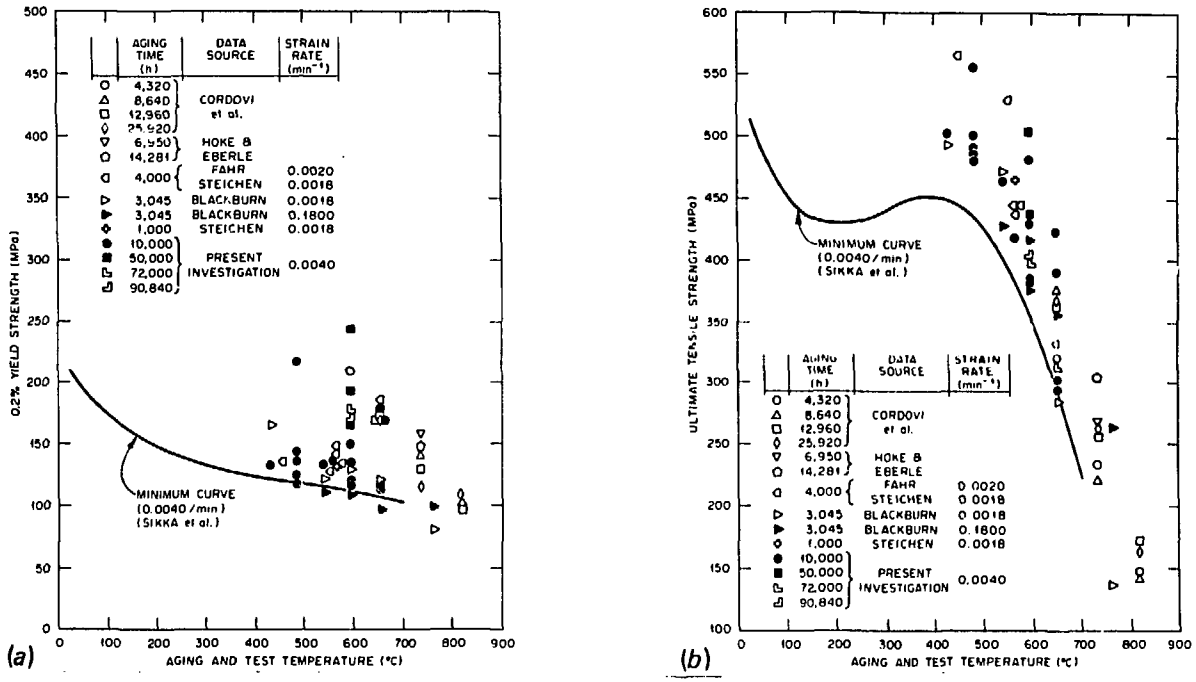

Fig. 3. Yield and ultimate strengths of type 316 stainless steel annealed after aging for up to 90,840 h (10.4 years). Sources of data: M. A. Cordovi et al., pp. 8–55 in *Behavior of Superheater Alloys in High Temperature, High Pressure Steam*, American Society of Mechanical Engineers, New York, 1968; J. Hoke and F. Eberle, *Trans. ASME* 79, 307–17 (1957); L. D. Blackburn, Hanford Engineering Development Laboratory, private communication to V. K. Sikka, 1975; J. M. Steichen, HEDL-TME 75-15, Hanford Engineering Development Laboratory, Richland, Wash., January 1975; D. Fahr, ORNL/TM-4292, Oak Ridge National Laboratory, Oak Ridge, Tenn., November 1973.

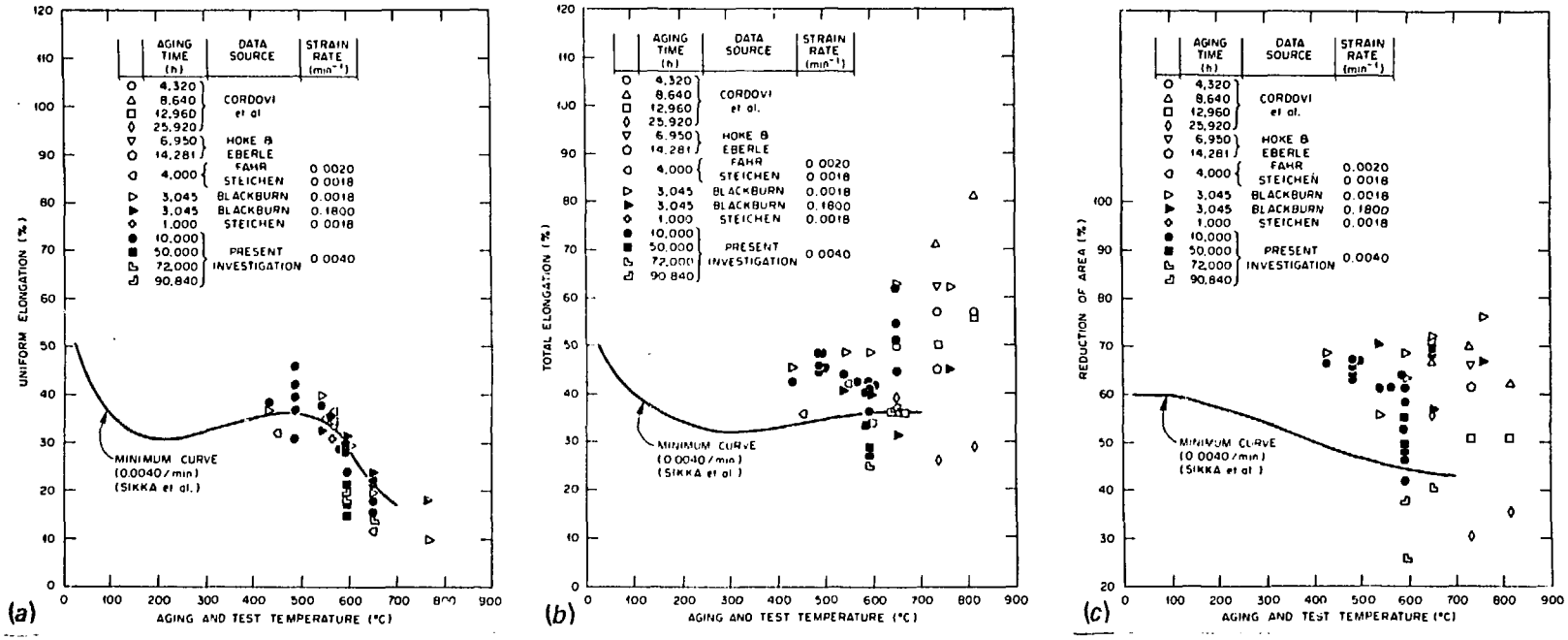

Fig. 4. Uniform and total elongation and reduction of area of type 316 stainless steel anealed after aging for up to 90,840 h (10.4 years). Sources of data: M. A. Cordovi et al., pp. 8–55 in *Behavior of Superheater Alloys in High Temperature, High Pressure Steam*, American Society of Mechanical Engineers, New York, 1968; J. Hoke and F. Eberle, *Trans. ASME* 79, 307–17 (1957); L. D. Blackburn, Hanford Engineering Development Laboratory, private communication to V. K. Sikka, 1975; J. M. Steichen, HEDL-TME 75-15, Hanford Engineering Development Laboratory, Richland, Wash., January 1975; D. Fahr, ORNL/TM-4292, Oak Ridge National Laboratory, Oak Ridge, Tenn., November 1973.

and 4 are for 12 aging times.[4,5] For the important temperature range of application for this steel in LMFBRs [500–625°C (930–1160°F)], the 0.2% yield and ultimate tensile strengths are either unaffected or increased by aging. From these data it is reasonable to state that no unforeseen decreases in strength will occur for unstressed material for service times between the 10.4 years (Figs. 3 and 4) and the 21 and 28 years of service required for LMFBRs with 30- and 40-year lifetimes at a capacity factor of 70%. At temperatures above 550°C (1022°F) precipitation reactions are essentially complete for this alloy for some of the times shown in Figs. 3 and 4, and a stable matrix and grain-boundary structure should be present. Ductility falls below the minimum for aging temperatures of 593°C (1100°F) and above. However, total elongation and reduction of area are still above 25%, which is quite acceptable for all anticipated out-of-core applications. Some implications of the lower ductility of aged material are discussed later under toughness properties.

In addition to knowledge of the effects of thermal exposure on the tensile properties of structural alloys, knowledge of the effects of prior load exposure is needed for extrapolation to conditions beyond laboratory tests. Figures 5 and 6 contain data on the effects of prior creep and fatigue loading, respectively, on the tensile properties of type 304 stainless steel.[3,6] At 538 and 593°C (1000 and 1100°F), strength and ductility properties decrease linearly as a function of prior creep strain. Prior creep strain of 0.17 to 0.18 produces a 20% decrease in ultimate tensile strength but a much larger decrease in ductility, as shown by the 50% decrease in total elongation.

Cyclic loading at 593°C (1100°F) and a total strain range of 0.4% had no effect on the tensile properties of type 304 stainless steel at this temperature, even for cycling to 75% of the fatigue life (cycles to failure). For total strain ranges of 1.0% the yield strength was increased by about 25%, and the ductility was decreased by about 25%, but the ultimate tensile strength was unaffected. Adding tensile hold times of 0.1 and 0.5 h in each cycle at the 1% strain range had no further effect on the yield or ultimate tensile strength, but the ductility decreased with increasing hold time. At 75% of the fatigue life the ductility was decreased almost 50% by a 0.1-h hold time and at only 50% of the fatigue life the ductility was reduced by a 0.5-h hold time to only 43% of that before the creep-fatigue loading. This information indicates that continuous-cycling fatigue loading at maximum strain ranges up to 1% at 593°C (1100°F) has little, if any, effect on the tensile properties of type 304 stainless steel. The data in Fig. 6 combined with the data shown in Fig. 5 illustrate that creep damage produced in either monotonic or cyclic loading is detrimental to these properties. The property affected most by creep loading is ductility. Discussion of this decrease in ductility is presented later under the toughness properties.

Creep-Rupture Properties

Figure 7 shows the forms of $Cr_{23}C_6$ precipitate particles in type 304 stainless steel after a creep-rupture test for 59,899 h at 593°C (1100°F) and 117 MPa.[7,8] The precipitate particles are large (50–100 nm across) and primarily rectangular. Figure 8 shows massive precipitates of sigma phase and fine precipitation of $Cr_{23}C_6$ in the same sample, and Fig. 9 shows that sufficient localized chromium depletion from the austenite during precipitation of sigma can result in the sigma being surrounded by δ-ferrite.

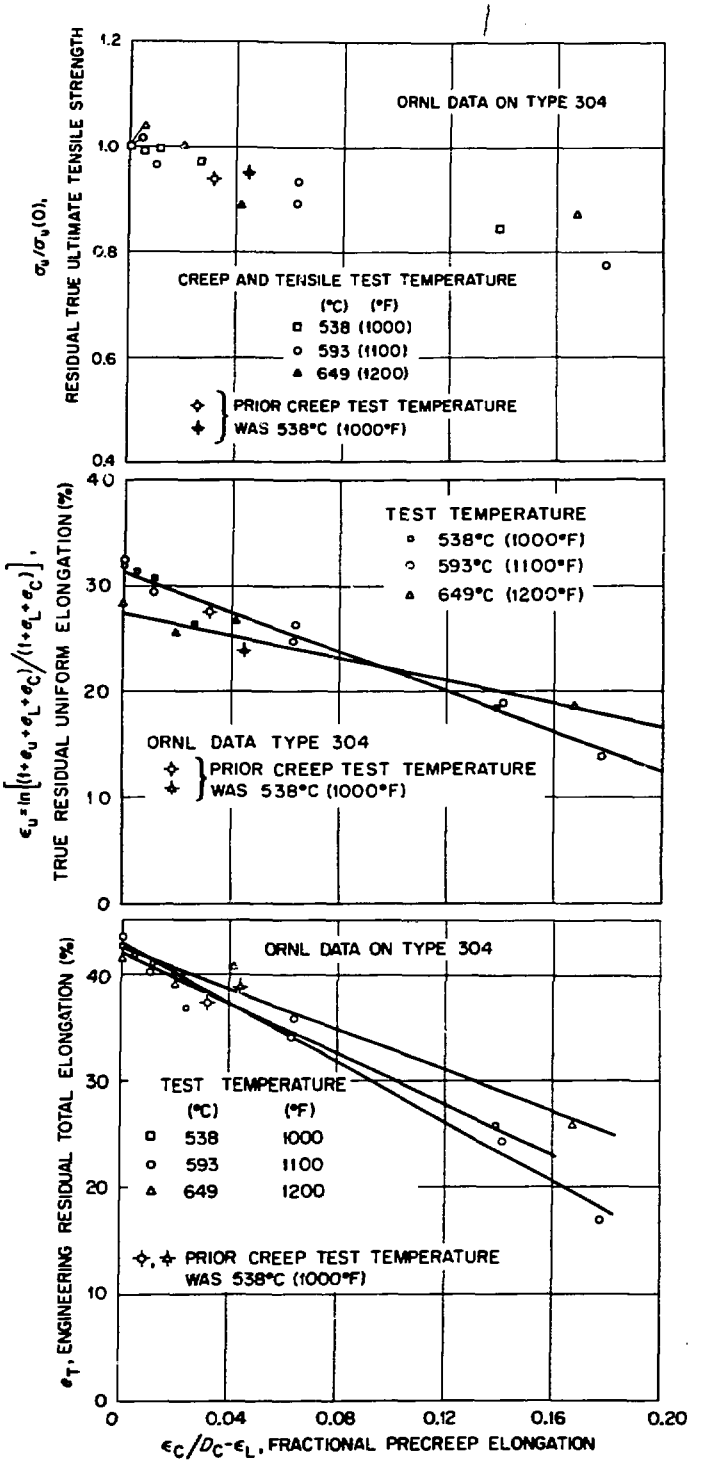

Fig. 5. Residual tensile properties of type 304 stainless steel at 538, 593, and 649°C (1000, 1100, and 1200°F) as a function of prior creep elongation.

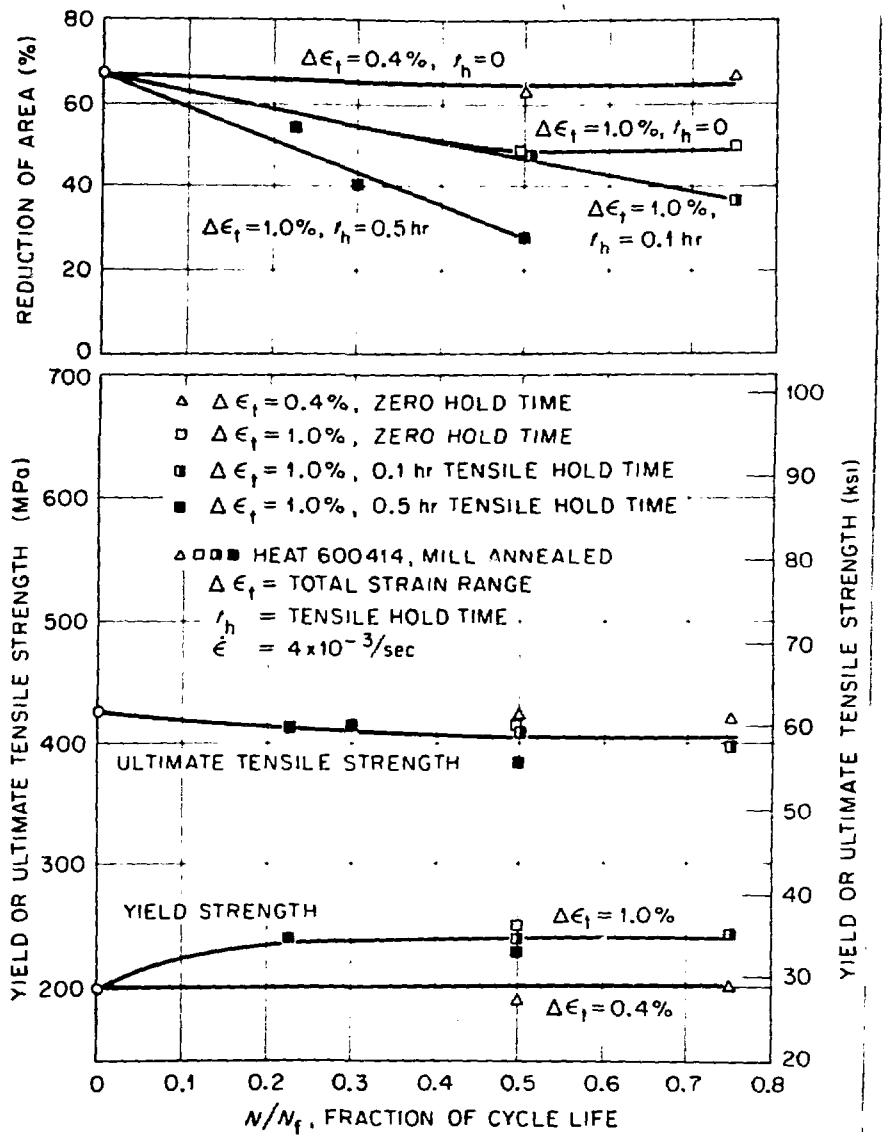

Fig. 6. Tensile properties as a function of cycle life expended for type 304 stainless steel cycled in strain control at 593°C (1100°F) (N_f = cycles to failure).

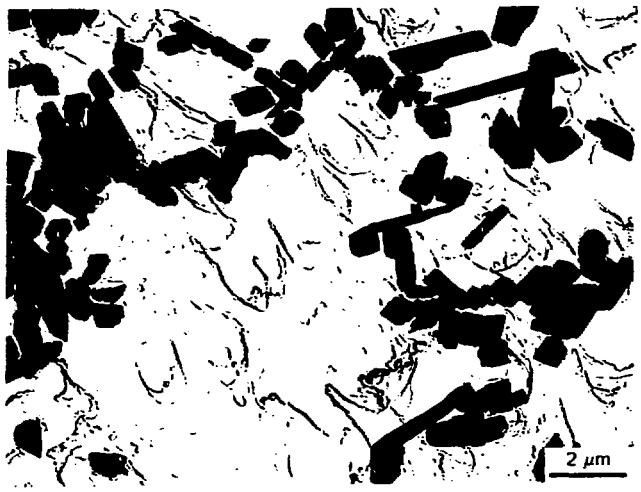

Fig. 7. Transmission electron micrograph of carbon extraction replica showing forms of $Cr_{23}C_6$ particles extracted from the stressed region of type 304 stainless steel after 59,899 h (6.8 years) at 593°C (1100°F) and 117 MPa.

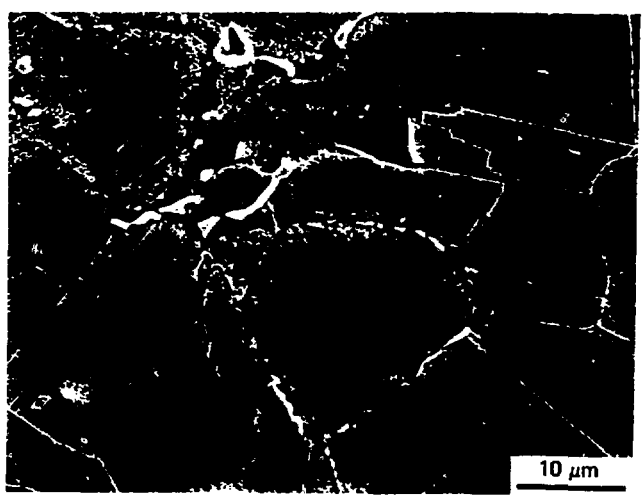

Fig. 8. Scanning electron micrograph showing massive sigma phase and fine particles of $Cr_{23}C_6$ precipitated in the stressed region of type 304 stainless steel during 59,899 h (6.8 years) at 593°C (1100°F) and 117 MPa.

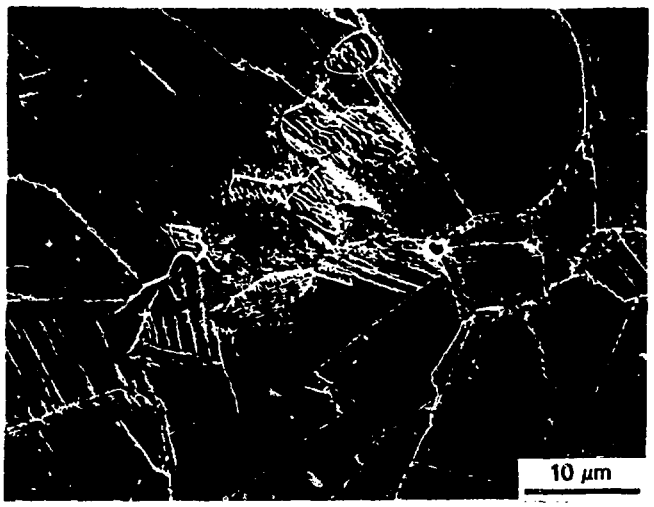

(a)

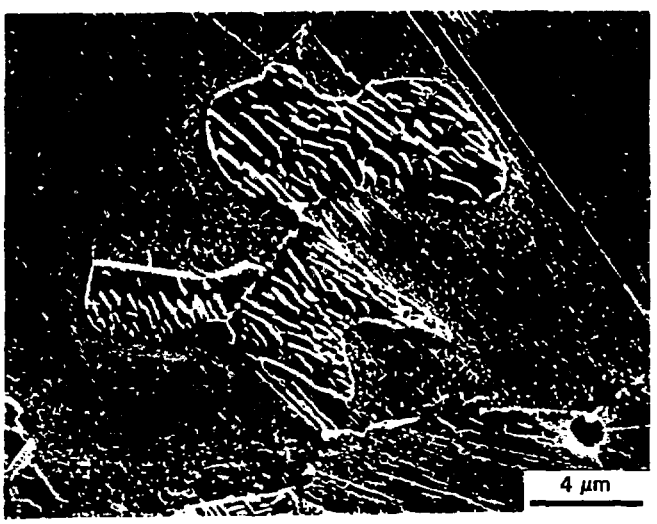

(b)

Fig. 9. Scanning electron micrograph showing large islands of δ-ferrite containing fine particles of sigma phase precipitated in the stressed region of type 304 stainless steel during 59,899 h (6.8 years) at 593°C (1100°F) and 117 MPa.

Figure 10 is an optical micrograph from a creep-rupture specimen that ruptured after 73,435 h (8.4 years) at 593°C (1100°F) and 117 MPa. At the center of the micrograph is evidence that the original grain boundary moved during the test. The matrix in this area is apparently void of any precipitates. They were dissolved during the grain-boundary movement under the applied stress. The grains contain an essentially uniform distribution of carbide particles, and massive sigma phase particles are found at grain-boundary intersections. Figures 7 through 10 are all in excellent agreement with the relatively short-term aging studies of Weiss and Stickler.[1] The information derived from these figures shows that the time-temperature-precipitation diagrams developed by Weiss and Stickler for types 304 and 316 stainless steel can be very effectively used to predict the microstructures and associated mechanical properties of these alloys for long-term testing and service conditions in the operation of LMFBRs.

Figure 11 contains data for the creep-rupture life for 11 heats of type 304 stainless steel tested at 593°C (1100°F) in this program and the minimum time to rupture curve for ASME Code Case N-47. Except for a few tests at 172 MPa the long-term creep-rupture properties for type 304 stainless steel are well above the ASME minimum for rupture lives up to 9.6×10^4 h.

Figure 12 shows the creep curves at 593°C (1100°F) and a stress of 172 MPa for type 316 stainless steel in the annealed condition and after aging for 10^4 h at 593°C (1100°F). This aging increased the secondary (steady-state) creep rate, rupture life, rupture ductility, and the time to onset of tertiary creep. The effects of a much longer aging time (4.4×10^4 h) on the creep rupture curves for type 316 stainless steel at 593°C (1100°F) are shown in Fig. 13 for stress of 207 MPa. At 172 MPa (same stress as in Fig. 12) aging for 4.4×10^4 h resulted in a large increase in secondary creep rate and a slight increase in ductility and in a slight decrease in the times to the onset of tertiary creep and rupture. For the higher stress of 207 MPa this aging resulted in a large increase in the secondary creep rate and ductility and in large decreases in the times to onset of tertiary creep and rupture. Note that aging increases creep ductility (low strain rates) but decreases tensile ductility (high strain rates).

Figure 14 shows log stress data versus the log creep rupture life at 593°C (1100°F) for type 316 stainless steel annealed and after aging for times up to 7.4×10^4 h (8.5 years) at temperatures from 482 to 649°C (900–1200°F). Also shown in Fig. 14 is the log of minimum strength versus log rupture life from ASME Code Case N-47. For all aging histories shown, the time to rupture for aged material exceeds that for the ASME minimum. Hence, long-term thermal exposures (~5 years) at temperatures up to 649°C (1200°F) and stresses too low to drastically alter the precipitation reactions do not shorten the subsequent creep-rupture life of type 316 stainless steel at temperatures up to 593°C (1100°F). As stated for the tensile properties, little or no further effects of aging on the creep-rupture properties are expected as a result of additional thermal exposures at low stresses for temperatures up to about 593°C (1100°F).[9]

Figures 15 and 12 show optical metallography from the annealed material and material aged for 10^4 h at 593°C (1100°F) and creep-rupture tested at 172 MPa at 593°C (1100°F). In annealed material the applied stress resulted in considerable grain-boundary cavitation [15(α)] and intergranular failure with little or no plastic deformation of the grains, but in aged material the same applied stress resulted in extensive plastic deformation of the grains and small ductile intragranular cavitation,

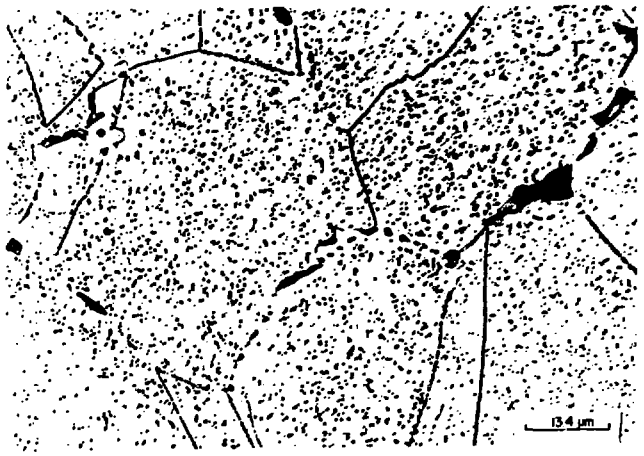

Fig. 10. Optical micrograph showing large amounts of carbide precipitation within the matrix and large sigma phase particles at the grain boundaries in the stressed region of type 304 stainless steel during 73,435 h (8.4 years) at 593°C (1100°F) and 117 MPa.

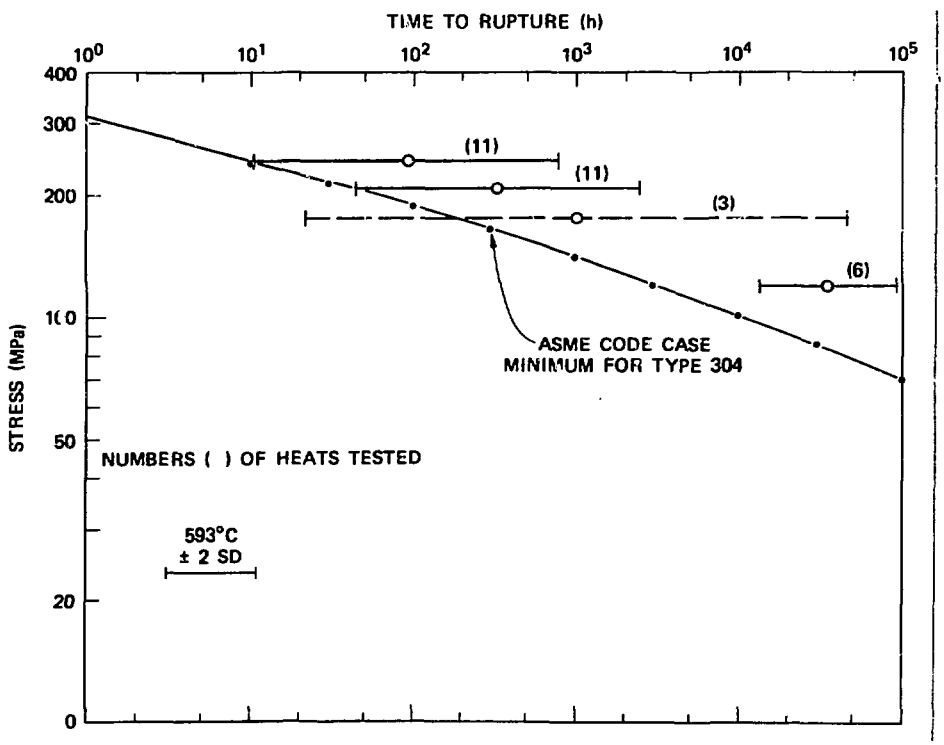

Fig. 11. Time to rupture as a function of applied stress at 593°C for 11 heats of type 304 stainless steel and ASME Code Case N-47 minimum for type 304 stainless steel at 593°C.

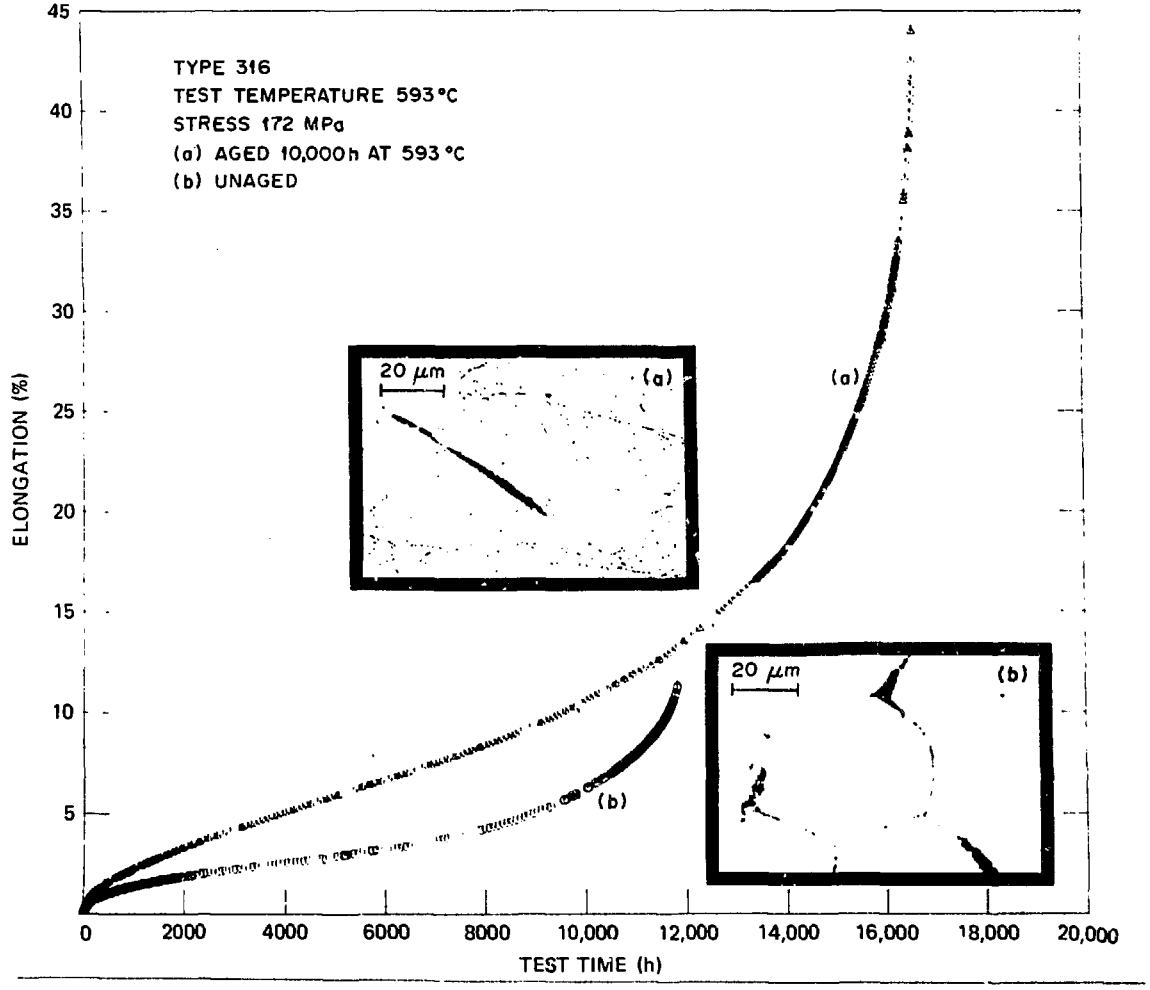

Fig. 12. Elongation as a function of test time at 593°C and 172 MPa and optical microstructures for type 316 stainless steel annealed and after aging for 10^4 h. The micrographs show (*a*) fine precipitate structure, intragranular deformation, and annealing twin crack in aged material and (*b*) lack of grain deformation and intergranular cracks in annealed material.

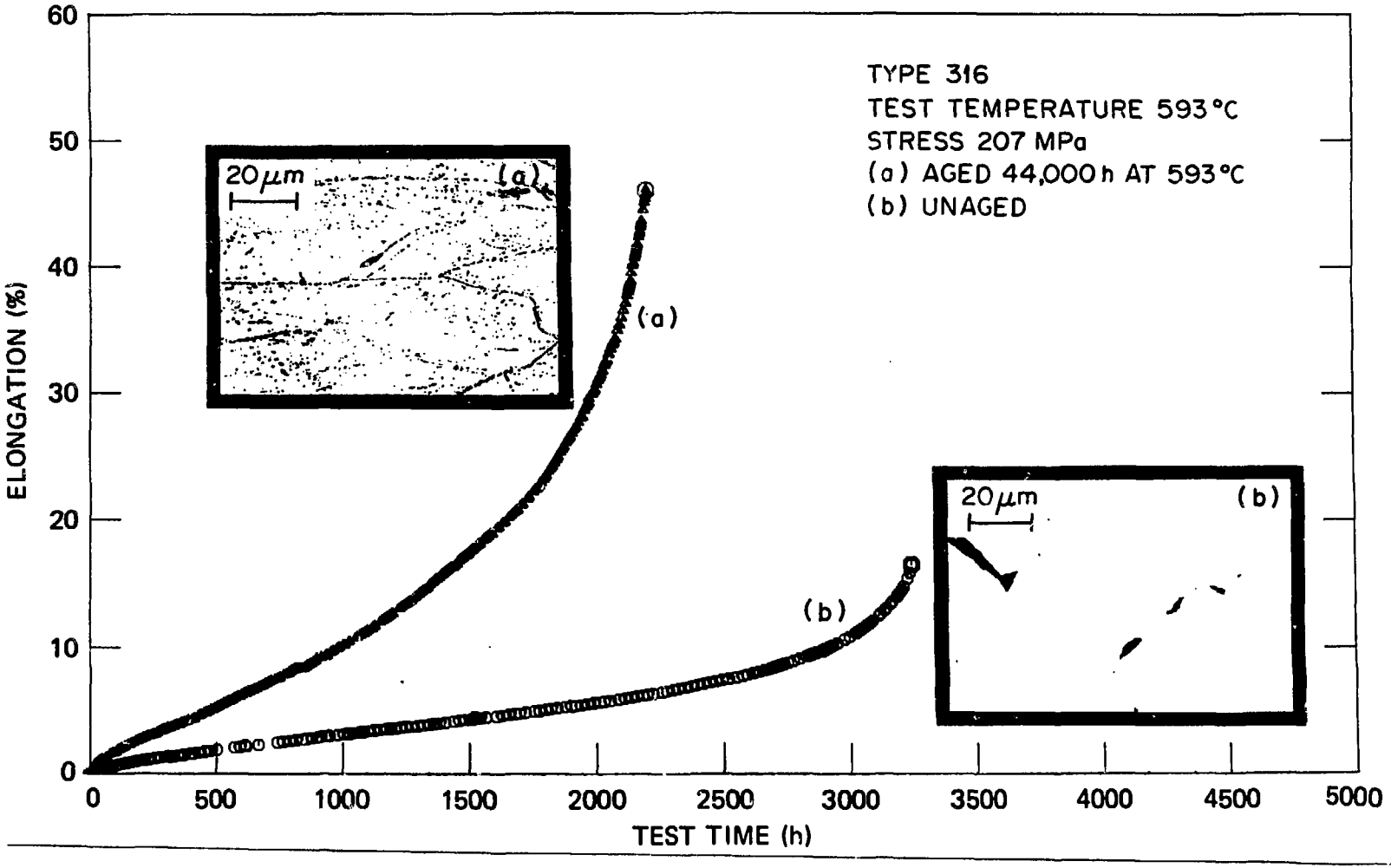

Fig. 13. Elongation as a function of test time at 593°C and 207 MPa and optical microstructures for type 316 stainless steel annealed and after aging for 4.4×10^4 h (5 years).

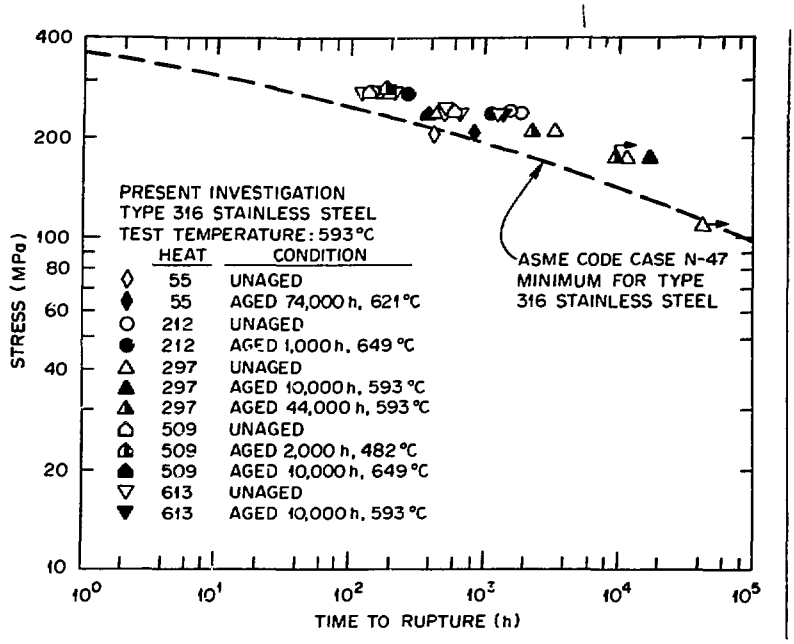

Fig. 14. Time to rupture as a function of stress at 593°C (1100°F) for type 316 stainless steel annealed and after aging for up to 7.4×10^4 h (8.4 years) and ASME Code Case N-47 minimum for type 316 stainless steel at 593°C (1100°F).

leading to ductile tearing with no observable grain-boundary cavitation or intergranular failure [15(*b*)]. The higher ductility and the associated benefits of the aged material compared with those of the annealed material are clearly evident in Fig 15. Figure 12, which includes micrographs at a much higher magnification than Fig. 15, shows the details of the microstructure and mode of failure for [Fig. 12(*a*)] the aged and [Fig. 12(*b*)] annealed materials. The annealed material has some precipitate particles at the grain boundaries but no precipitation within the grains. Intergranular cavitation and cracking are the dominant modes of failure. The aged material has many small precipitate particles at the grain boundaries and within the grains. For this microstructure, deformation of grains and nucleation of cracks at annealing twins are the dominant mode of deformation and failure.[10] Precipitation during aging has strengthened the grain boundaries relative to annealed material and has thereby eliminated intergranular cavitation and fracture, resulting in longer creep-rupture life.

Figure 16 provides similar information for this alloy aged 4.4×10^4 h at 593°C and creep-rupture tested at 593°C (1100°F) and 207 MPa. The most important aspects of Fig. 16 are that the precipitate structure and deformation mode in the aged material have not changed from that shown in Fig. 12(*a*), which was aged for 10^4 h before testing at a slightly lower stress. This provides further evidence for the desired stability of the aged structure for elevated-temperature applications in LMFBRs.

Figure 17 shows the sigma phase precipitate present in type 316 stainless steel after 1.25×10^5 h (11.4 years) of service at 621°C (1150°F)

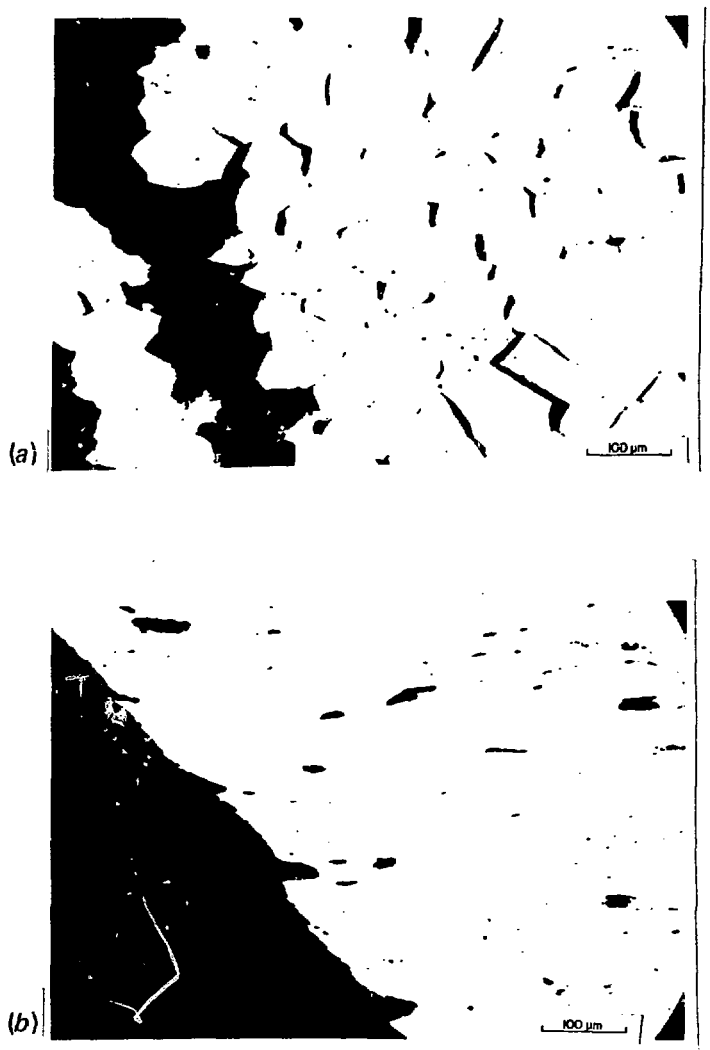

Fig. 15. Fracture behavior of type 316 stainless steel creep-rupture tested at 593°C (1100°F) and 172 MPa. (*a*) Annealed; extensive intergranular cracking with large cavities and no intragranular deformation. (*b*) Aged for 10^4 h at 593°C (1100°F); considerable intragranular deformation with few small to medium-size cavities.

Fig. 16. Optical micrograph of type 316 stainless steel aged for 4.4×10^4 h at 593°C (1100°F) before creep testing. Precipitate structure and mode of failure are the same as for material aged for 10^4 at 593°C (1100°F) shown in Fig. 12.

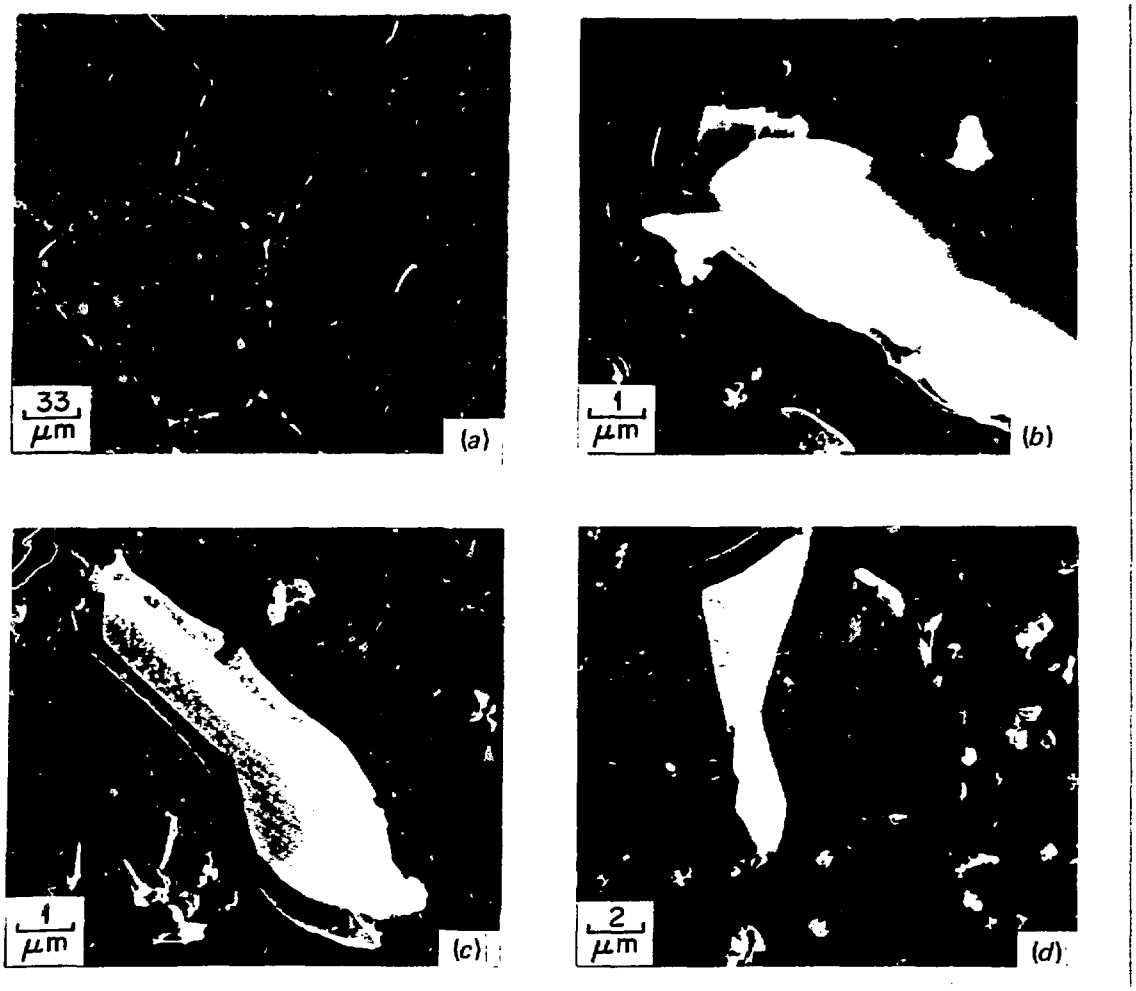

Fig. 17. Scanning electron micrographs of type 316 stainless steel pipe after 1.25×10^5 h (14.3 years) of service at 621°C (1150°F). (*a*) Overview. (*b*) Laminated structure of large sigma phase particles shown in the grain boundaries of (*a*). (*c*) Delamination of sigma phase particles and matrix precipitate. (*d*) Delamination of another sigma phase particle and additional matrix precipitate.

(ref. 4) and is very consistent with the analysis of Weiss and Stickler.[1] Although this temperature is well above that anticipated for type 316 stainless steel for out-of-core applications, testing at lower temperatures must be continued to determine if similar structures will be produced by longer exposures at lower temperatures combined with LMFBR operating stresses.

Fatigue and Creep-Fatigue Properties

Figures 18 through 20 show the effects of shorter term aging on the cyclic creep-fatigue lifetimes and microstructures of type 316 stainless steel at 550°C (1022°F). All three figures show the same plots of log strain range against log fatigue life; however, each of these figures shows a different and important aspect of the microstructures associated with the different fatigue lines. The dashed curve is the log of strain range versus the log of fatigue life for continuous cycling. For annealed material (curve *a*) a tensile hold period of 0.5 h during each cycle reduces

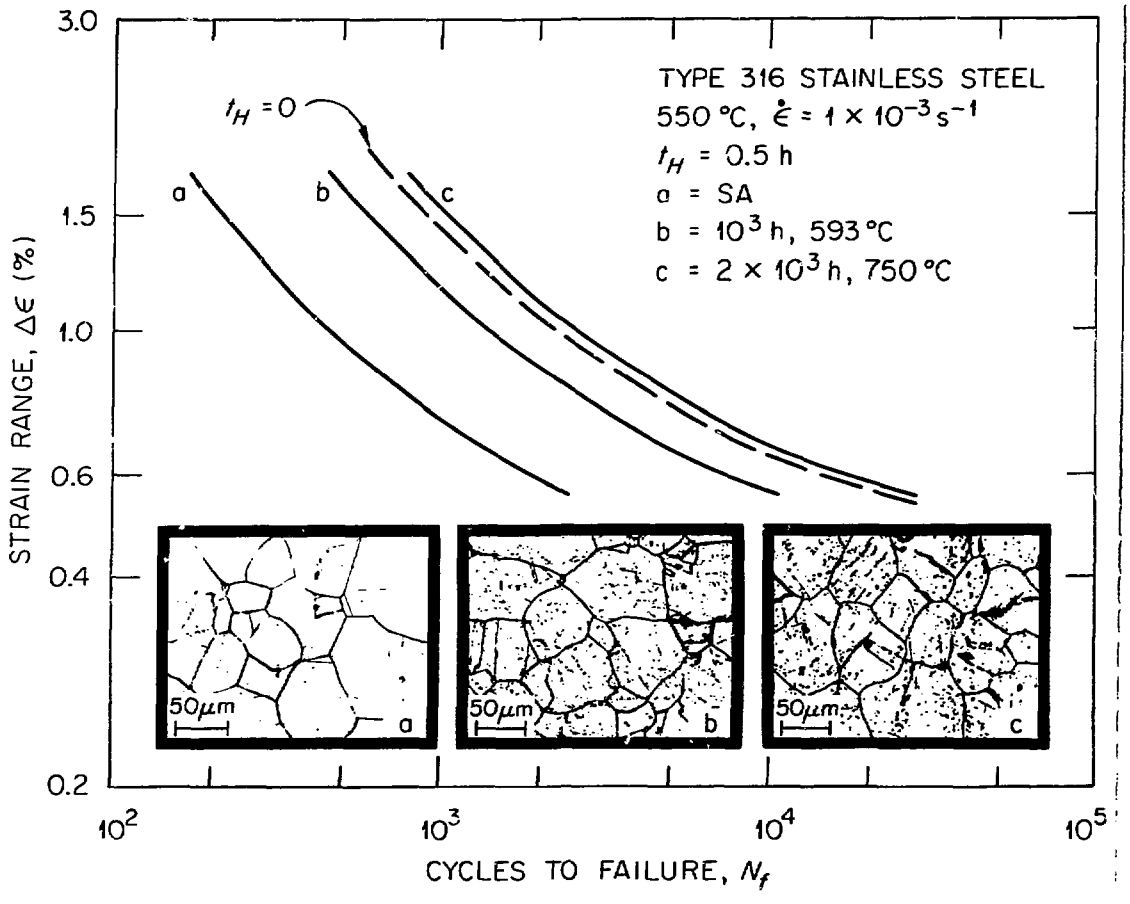

Fig. 18. Cycle life N_f as a function of strain range for cyclic creep-fatigue of type 316 stainless steel at 550°C (1022°F) and optical micrographs for material (*a*) as annealed, (*b*) aged for 10^3 h at 593°C (1100°F) and, (*c*) aged for 2×10^3 h at 750°C (1382°F). Dashed line is for continuous cycling fatigue with no hold time.

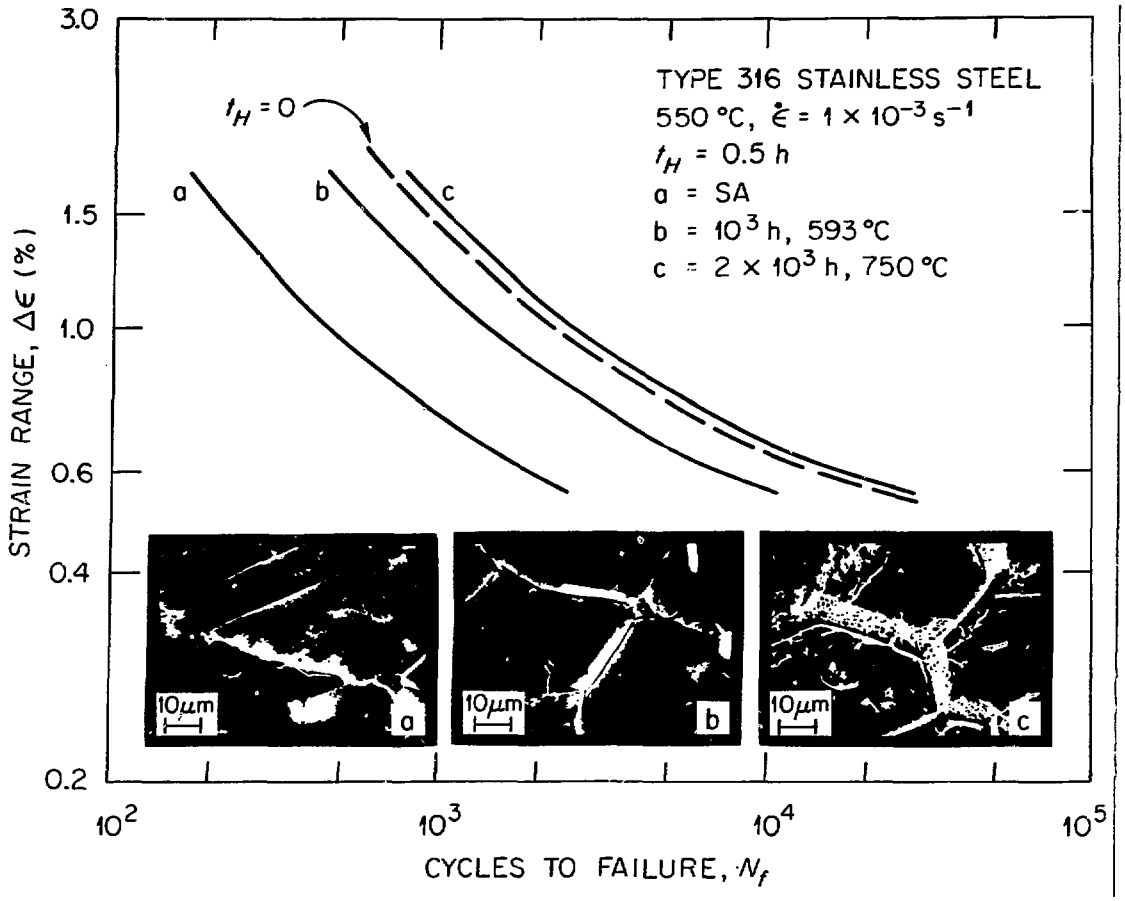

Fig. 19. Cycle life N_f as a function of strain range for cyclic creep-fatigue of type 316 stainless steel at 550°C (1022°F) and scanning electron micrographs for material (*a*) as annealed, (*b*) aged for 10^3 h at 593°C (1100°F), and (*c*) aged for 2×10^3 h at 750°C (1382°F). Dashed line is for continuous cycling fatigue with no hold time.

the creep-fatigue life to only one-fourth that for continuous cycling. Aging for 10^3 h at 593°C (1100°F) (curve *b*) improves the creep-fatigue life to approximately two-thirds of that for continuous cycling. Aging for 2×10^3 h at 750°C (1382°F) (curve *c*) improves the creep-fatigue life to almost 25% greater than that for continuous cycling and more than 4 times that for unaged material under the same test conditions. Aging also improved the continuous-cycling fatigue life, but the magnitude of the improvement is not as great as that for the creep-fatigue life.

The microstructure is shown by optical microscopy in Fig. 18. The annealed material (*a*) shows a small amount of precipitation ($M_{23}C_6$) at the grain boundaries and very little observable precipitation within the grains. In (*b*) more precipitation occurs at the grain boundaries, and precipitation is observable at annealing twin boundaries and other sites within the grains. In (*c*) more massive precipitation is seen at the grain

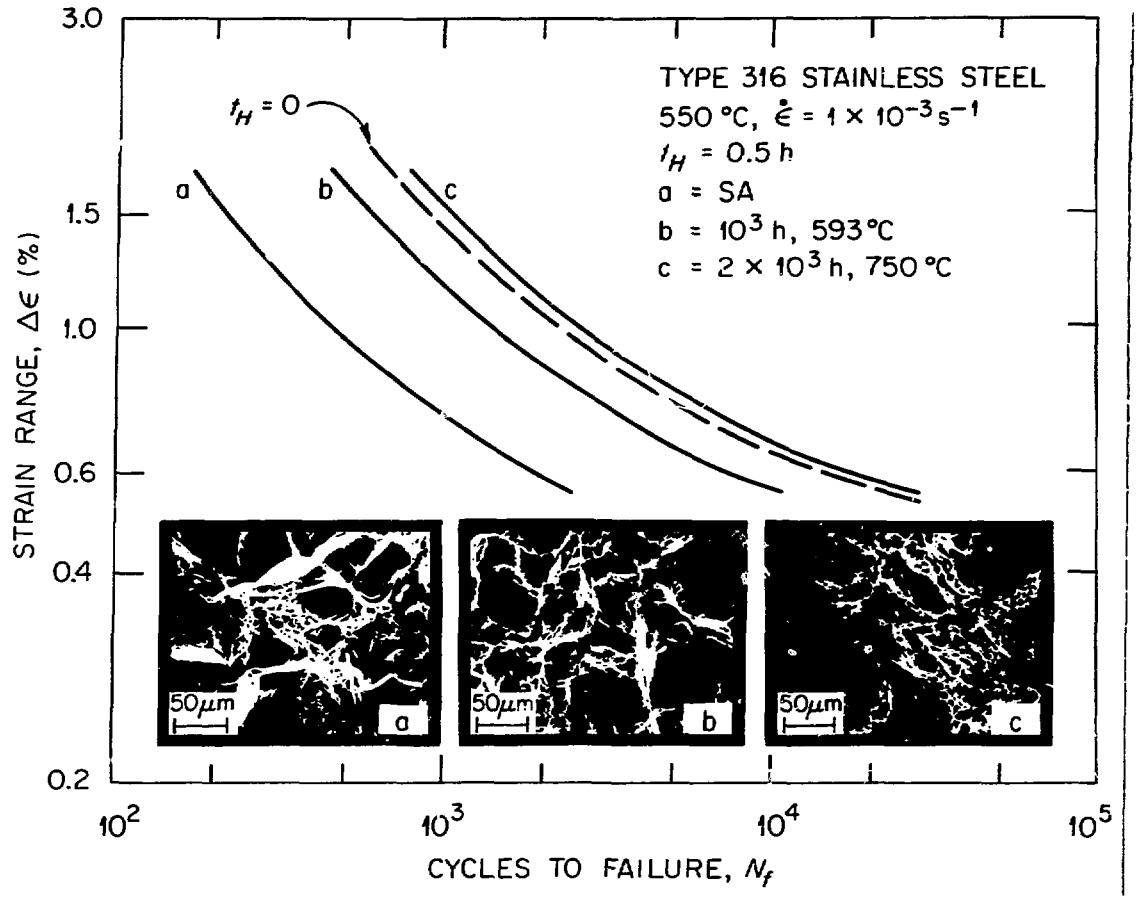

Fig. 20. Cycle life N_f as a function of strain range for cyclic creep-fatigue of type 316 stainless steel at 550°C (1022°F) and scanning electron fractographs for material (*a*) as annealed, (*b*) aged for 10^3 h at 593°C (1000°F), and (*c*) aged for 2×10^3 h at 750°C (1382°F). Dashed line is for continuous cycling fatigue with no hold time.

boundaries and within the grains, and the intragranular precipitate particles appear to be larger than in (*b*). Figure 19 shows scanning electron microscopy for material having the creep-fatigue lives shown by curves *a*, *b*, and *c*. The amount of grain-boundary precipitate increases by large increments during aging, as shown in micrographs (*a*), (*b*), and (*c*). This figure clearly shows that the increase in creep-fatigue life on aging is due to the alteration of the grain-boundary and matrix structure by the precipitation.

Figure 20 shows scanning electron fractography associated with creep-fatigue curves (*a*), (*b*), and (*c*). For annealed material (*a*) fracture is intergranular with very little evidence of ductile behavior. For (*b*) intergranular failure is combined with some ductile tearing. In (*c*) the fractograph indicates that failure was totally by intragranular ductile tearing, with no evidence of brittle intergranular failure. As discussed earlier, alteration of the grain-boundary and matrix microstructure by

these precipitates reduces or eliminates grain-boundary cavitation and cracking during creep loading and thereby improves the creep-rupture and creep-fatigue properties.

Toughness Properties

The Charpy impact properties of austenitic stainless steels are not measured or cited very often because these steels do not lose fracture toughness or change from ductile to brittle behavior at low temperatures. However, as shown in Fig. 21(*a*), prolonged elevated-temperature exposure of type 316 stainless steel can result in room-temperature Charpy impact strength values that are less than 10% of that for material in the annealed and unaged condition. Data in Fig. 21(*a*) are for both laboratory test specimens and material taken from actual power plant components. Recall that, as shown in Figs. 2 through 6, ductility is the property that is affected most by prior creep or fatigue loading or by thermal exposure for type 316 stainless steel under tensile loading (relatively high strain rate). This decrease in ductility under tensile test conditions is further manifested in the Charpy impact strength. Charpy impact strength values for type 316 stainless steel weldments with type 16-8-2 weld alloy agree reasonably well with those for base metal, as shown in Fig. 21(*b*). For the time, temperature, and stress conditions shown in Fig. 21(*b*), the Charpy impact properties of the weld metals are superior to those of the base metal. Work is in progress to attempt to relate the room-temperature Charpy impact properties with the elevated-temperature slower strain rate properties of these materials. This is not considered a concern for LMFBR systems because room-temperature Charpy impact values exaggerate the decrease in elevated-temperature toughness on aging and because LMFBR systems are not exposed to temperatures below refueling temperatures of at least 205°C (400°F), until shutdown at the end of the plant lifetime for decommissioning.

WELD METALS

The development of austenitic stainless steel welds with improved mechanical properties has been an objective of this program and the LMFBR programs of other nations. The American Society of Mechanical Engineers (ASME) imposes a strain limitation for all welded structures that operate at temperatures so high that creep can occur. Strain accumulation in the weld is restricted to one-half that in the base metal. In an attempt to reduce the strain limits in welded structures of austenitic stainless steels, the role of trace elements in the mechanical properties of types 308, 316, and 16-8-2 stainless steel weld metals was studied. Boron, phosphorus, and titanium each improves the elevated-temperature mechanical properties of these weld metals; however, maximum improvement in properties occurs when small concentrations of the three of these elements are combined at controlled concentrations in these alloys.[11-13] Weld materials containing controlled concentrations of these elements are referred to as controlled residual element (CRE) alloys. The composition that is currently used to improve the mechanical properties of these alloys is 0.002 to 0.008 wt % B, 0.03 to 0.05 wt % P, and 0.35 to 0.80 wt % Ti.[11-13]

Figure 22 shows the improvement in creep rupture life for types 308, 316, and 16-8-2 CRE stainless steel weld metals relative to the standard alloys. For all tests the rupture lives of CRE welds exceed those of the

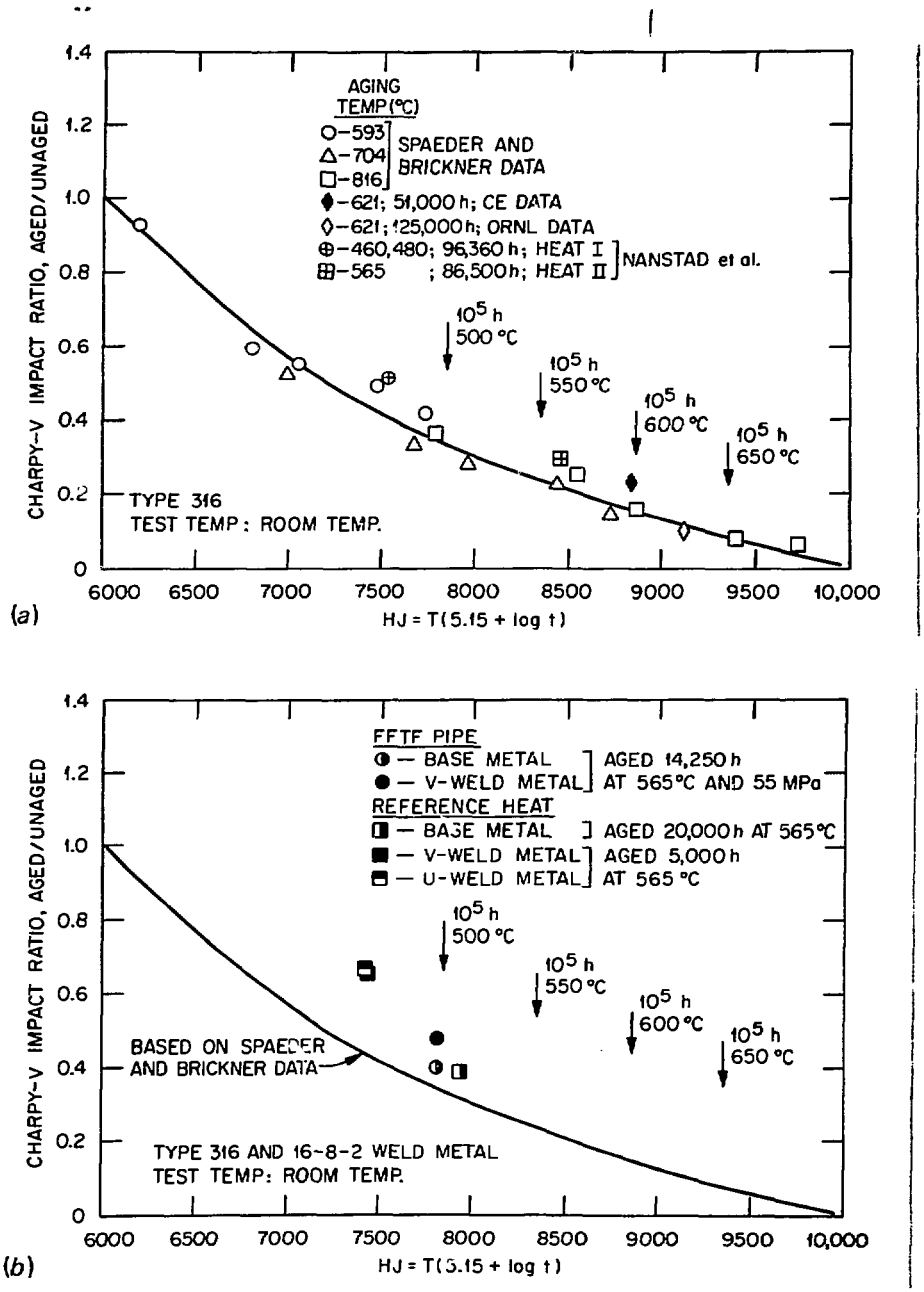

Fig. 21. Room-temperature Charpy impact strength as a function of Holloman-Jaffe parameter for (*a*) type 316 stainless steel after thermal aging or in-service exposure and (*b*) 16-8-2 weld metal after aging for up to 2 × 10^4 h at 565°C (1050°F). Unpublished data from ORNL and from Combustion Engineering, Inc., Chattanooga, Tenn., are compared with data of C. E. Spaeder, Jr., and K. G. Brickner, pp. 143–50 in *Advances in the Technology of Stainless Steels and Related Alloys*, ASTM STP 369, American Society for Testing and Materials, Philadelphia, 1965.

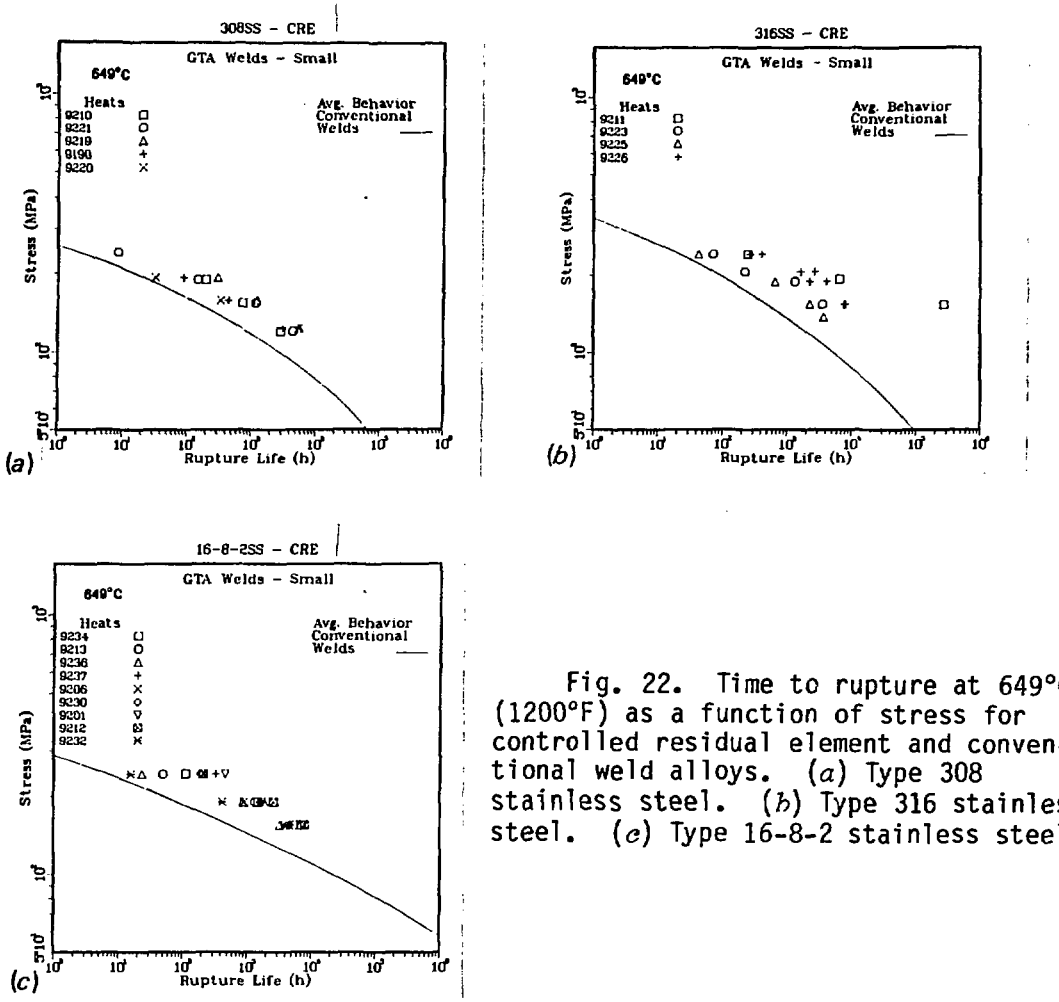

Fig. 22. Time to rupture at 649°C (1200°F) as a function of stress for controlled residual element and conventional weld alloys. (*a*) Type 308 stainless steel. (*b*) Type 316 stainless steel. (*c*) Type 16-8-2 stainless steel.

standard alloy. Figure 23 shows that CRE provides a significant improvement in rupture life at 649°C (1200°F) for the 16-8-2 weld metal. Also shown in Fig. 23 are microstructures of (*a*) gas tungsten arc (GTA) type 16-8-2 CRE weld metal and (*b*) GTA type 16-8-2 standard commercial weld metal. The microstructure of the CRE weld is much more uniform and on a much finer scale than that for the standard commercial weld metal. Figure 24 shows the microstructure of (*a*) CRE and (*b*) commercial 16-8-2 weld metal tested under the same conditions. The standard weld metal has a coarse dendritic microstructure with extensive cracking predominantly at the interfaces between austenite and δ-ferrite. The microstructure in the CRE weld metal is much finer and free of cracks.

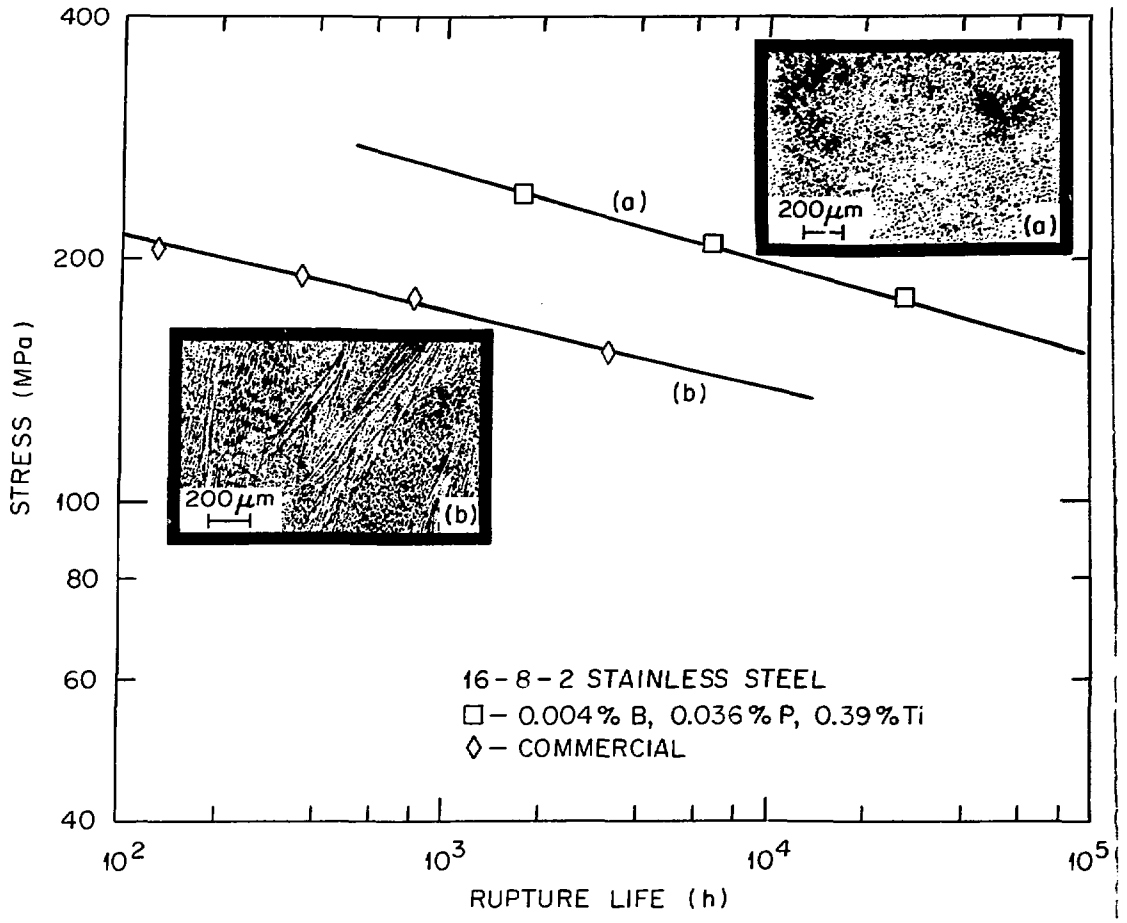

Fig. 23. Time to rupture as a function of stress at 649°C (1200°F) and associated optical microstructures for commercial and controlled residual element gas tungsten arc type 16-8-2 welds.

Figure 25 shows the minimum rupture life versus applied stress for GTA and submerged arc (SA) CRE welds and standard welds. These are calculated by the ASME procedure for base metals. For all three weld metals the CRE is superior. Figure 26 shows the ASME Code Case N-47 stress-rupture reduction factors for commercial 16-8-2 weld metal at 454, 538, and 593°C (850, 1000, and 1100°F) and the proposed stress-rupture reduction factor for 16-8-2 CRE for temperatures up to 593°C (1100°F). For CRE no reduction from unity is required for times up to 2×10^4 h, and tests are under way to extend this to times of 10^5 h and beyond. These data represent a valuable and significant contribution to the development of austenitic stainless steel filler metals and weldments with improved mechanical properties.

CAST MATERIALS

In addition to the development of filler metals and weldments with improved mechanical properties, the U.S. LMFBR Materials and Structures

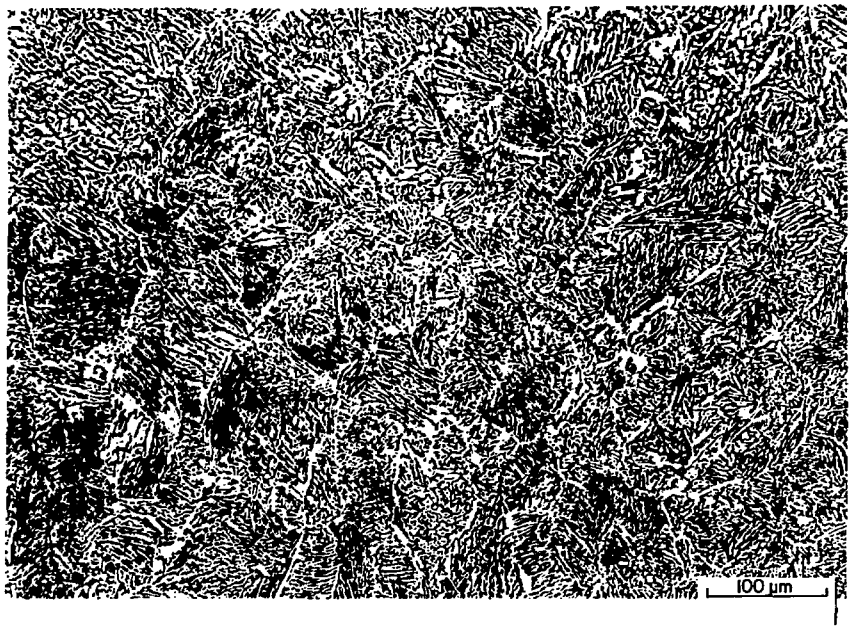

(a)

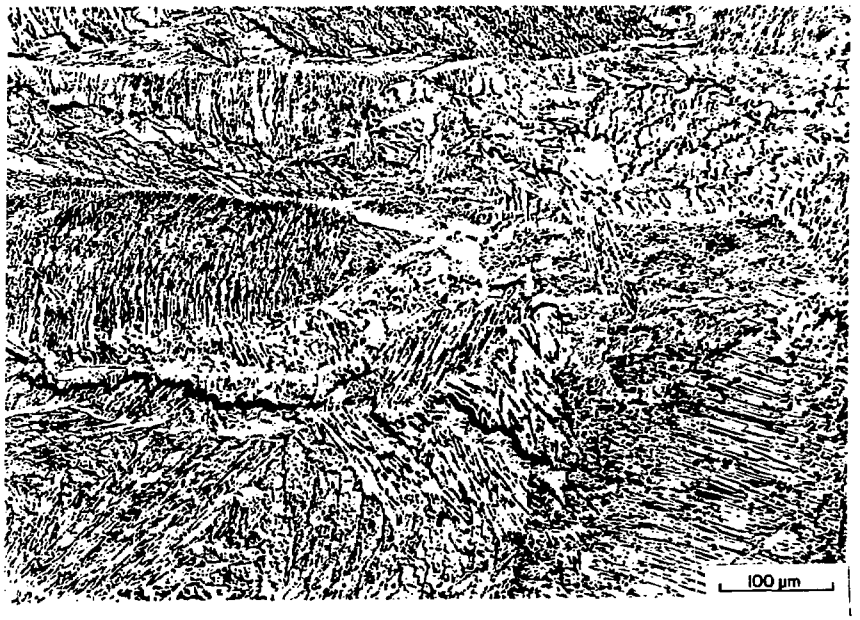

(b)

Fig. 24. Optical micrographs showing (*a*) fine equiaxed structure of controlled residual element 16-8-2 weld alloy and (*b*) coarse ansotropic structure with extensive cracking of commercial 16-8-2 weld alloy.

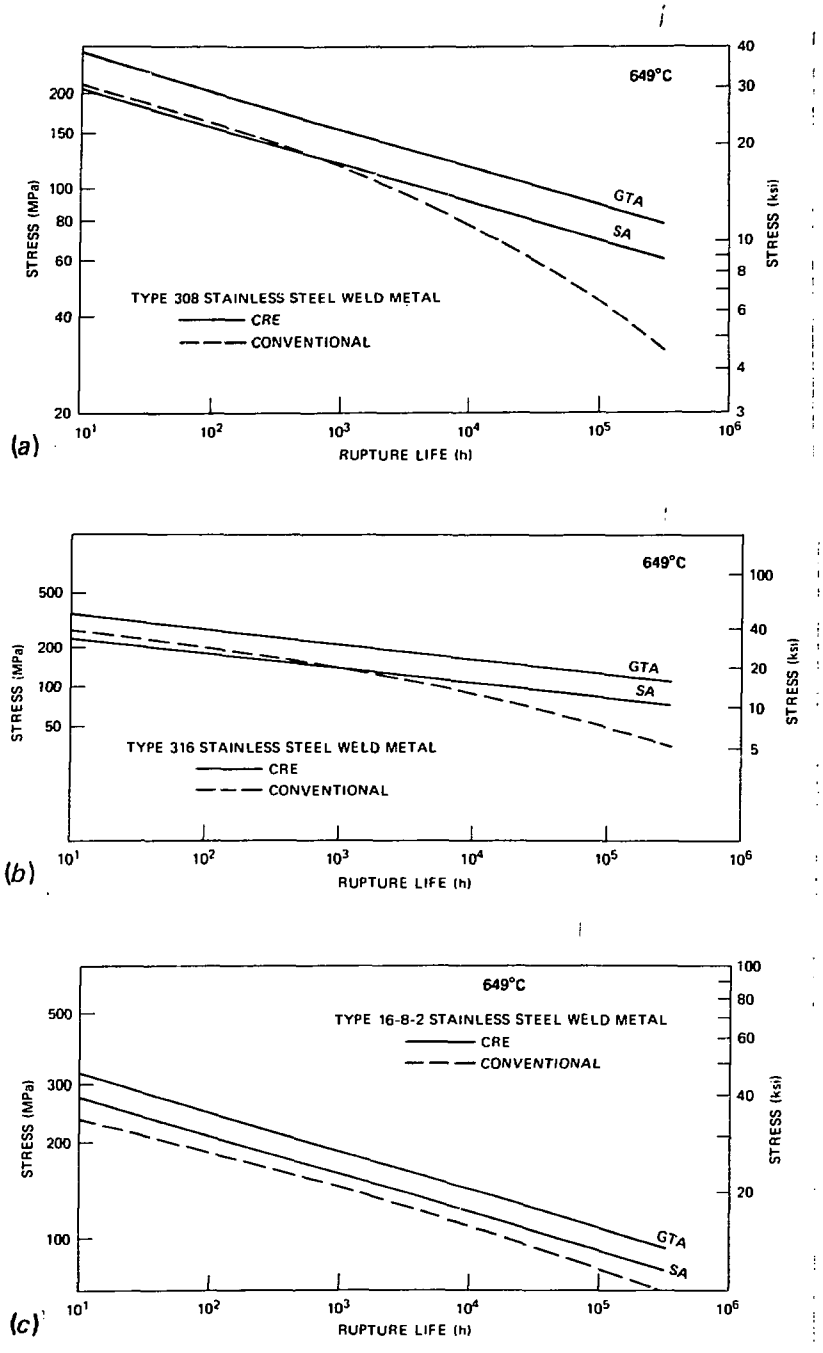

Fig. 25. Time to rupture as a function of applied stress at 649°C (1200°F) for conventional and controlled residual element submerged arc (SA) and gas tungsten arc (GTA) welds. (*a*) Type 308 stainless steel. (*b*) Type 316 stainless steel. (*c*) Type 16-8-2 stainless steel.

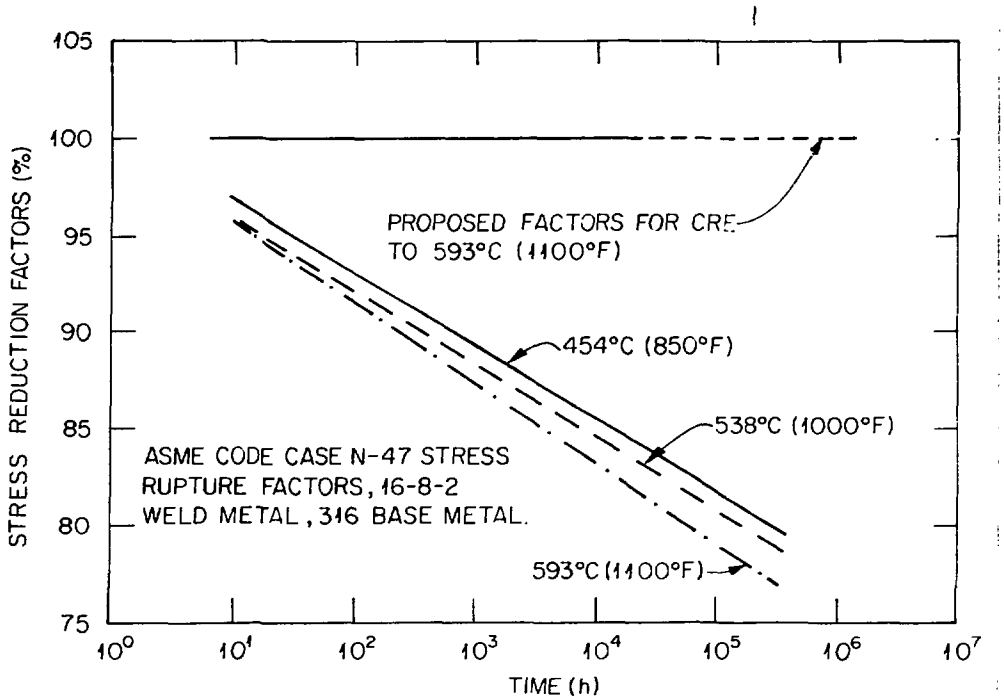

Fig. 26. Stress reduction factors for ASME Code Case N-47 for 16-8-2 controlled residual element and commercial 16-8-2 weld metals for temperatures up to 593°C (1100°F).

Program of Mechanical Properties for Design Data has equal emphasis on the mechanical behavior of castings of types 304 and 316 stainless steel, CF8 and CF8M, respectively. Castings of these two alloys have been used for core lower internal structures and for several components of sodium pumps for LMFBRs. For some components, such as pump impellers, the use of cast material is the only feasible method for producing complex geometries.

The mechanical properties of CF8 and CF8M are very sensitive to the δ-ferrite content and morphology in these materials.[14-16] The initial thermodynamic states and microstructures of these castings are extremely unstable when exposed to temperatures above about 350°C.[14-16] The δ-ferrite present in the original cast material has a very large influence on the mechanical properties of these materials for times up to the design lifetimes of the power plants in which they are used. During service exposure to temperatures above 538°C (1000°F) the δ-ferrite transforms to sigma phase and austenite. At lower temperatures it transforms to austenite and alpha prime, which is a chromium-rich (~26% Cr) phase.[14-16] Both sigma and alpha prime phases reduce the ductility of CF8 and CF8M. The ferrite content and morphology present in the initial cast structure determine the distribution and geometry of the resulting sigma or alpha prime phases and

austenite produced during elevated-temperature exposure. Recall that formation of sigma phase results in large decreases in the toughness properties of austenitic stainless steels.[1] Sigma and alpha prime phases have a much larger detrimental effect on mechanical properties when they are acicular or form continuous or semicontinuous networks within the austenite than when they are present as isolated globules. High initial ferrite contents (>15%) and very large ferrite islands in the original cast structure result in mechanical properties that are inferior to those of castings with low (5–12%) initial ferrite contents and small isolated ferrite islands.

To avoid the uncontrolled transformation of ferrite to sigma phase and austenite during power plant operation, most castings are given a dimensionally stabilizing heat treatment before use at elevated temperatures. The heat treatments are called dimensionally stabilizing because the transformation from the less dense ferrite to sigma phase and denser (close-packed structure) austenite densifies the casting. This densification results in dimensional changes in the casting. The magnitude of the dimensional decrease of the casting is proportional to the initial ferrite content of the casting and the amount of stress relaxation that occurs during the heat treatment.

Determination of the effects of initial ferrite content and morphology on the mechanical properties of CF8 and CF8M for applications in LMFBR components is a high-priority task within the current Materials and Structures Program. Measurements are in progress to determine the effects of long-term (10^4 to 5×10^4 h) aging and of dimensionally stabilizing heat treatments on the tensile, creep-rupture, fatigue, and fracture mechanics properties of CF8 and CF8M.

Figure 27 shows the microstructure and microhardness indention marks in CF8M with a ferrite content of 20 to 25% (*a*) in the as cast condition, (*b*) after 168 h at 482°C (900°F), and (*c*) after 24 h at 732°C (1350°F). In Fig. 27(*a*) the austenite appears white and the δ-ferrite appears gray. Note the small difference in hardness between the austenite and ferrite as shown by the size of the hardness indentation. Figure 27(*b*) shows very large increase (77%) in the hardness of the ferrite, with no observable change in its microstructure; the structure and hardness of the austenite remain approximately constant. Figure 27(*c*) shows an observable change in the microstructure of the ferrite, and its hardness is a little less than that shown in (*b*); again the structure and hardness of the austenite exhibit little change.

The room-temperature Charpy impact strength of this material was measured in the as-cast condition and after the dimensionally stabilizing heat treatment given the material shown in Fig. 27(*c*). Table I contains the Charpy impact values for the two thermodynamic states. The dimensionally stabilizing heat treatment has resulted in a severe embrittlement of the casting with a decrease in the Charpy impact strength from an average of 381 to 12 J (207–9 ft-lb). This is consistent with the 80% reduction in Charpy impact properties observed by Landerman and Bamford after aging of CF8M (ref. 14). Testing is under way to measure the effects of dimensionally stabilizing heat treatments on the other mechanical properties of CF8M.

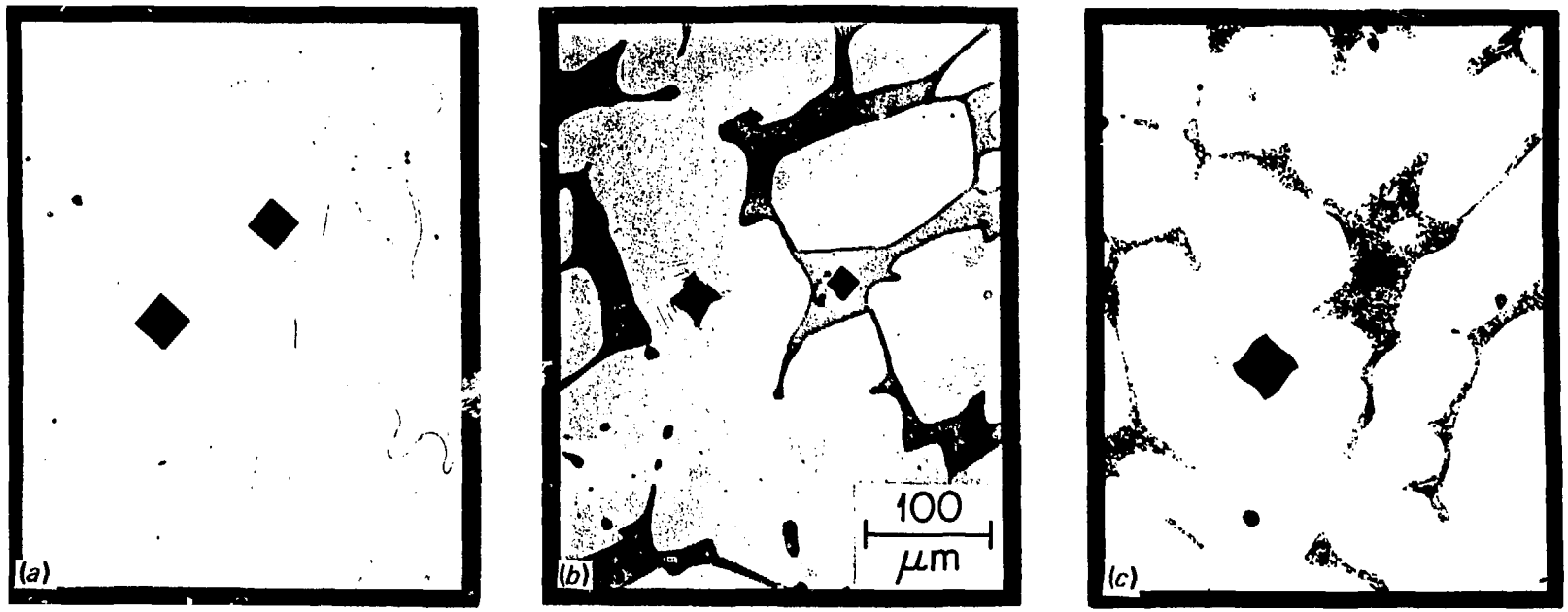

Fig. 27. Optical micrographs showing austenite, δ-ferrite, and microhardness indentions in CF8M. (*a*) As Cast. (*b*) After 168 h at 482°C. (*c*) After 24 h at 732°C.

Table I. Decrease in room-temperature Charpy impact strength due to heat treatment of CF8M

Charpy impact energy			
As cast		Heat treated at 732°C for 24 h	
(J)	(ft-lb)	(J)	(ft-lb)
Longitudinal			
261	192	8	6
277	204	9.5	7
267	195	12	9
Transverse			
245	180	15	11
268	197	11	8
272	200	18	13
Thickness			
326	240+	9.5	7
295	217	13.5	10
317	233	12	9

SUMMARY

The long-term mechanical properties of types 304 and 316 stainless steel can be correlated with the microstructures that are produced during elevated-temperature testing and/or service exposure relevant to LMFBR application. The information presented in this paper supports the following conclusions.

- Long-term aging (up to 91,000 h so far) at temperatures up to about 600°C (1100°F) has no detrimental effect on the tensile strength of type 316 stainless steel.
- This long-term aging decreases the ductility of type 316 stainless steel; however, after 91,000 h at 649°C (1200°F) the ductility is still adequate for any anticipated out-of-core applications.
- Creep loading before tensile loading reduces the tensile properties.
- Fatigue loading before tensile loading has no effect on the tensile properties, but cyclic creep-fatigue loading reduces tensile ductility.
- Long-term aging produces $M_{23}(C,N)_6$, sigma phase, and δ-ferrite in types 304 and 316 stainless steel in accordance with the analysis of Weiss and Stickler. Therefore, precipitation and phase stability data may be used to predict long-term behavior of these alloys for LMFBR service.
- For long-term testing and aging (~96,000 h so far) of types 304 and 316 stainless steel, the times to rupture as a function of applied stress exceed the minimum for ASME Code Case N-47.
- For type 316 stainless steel, aging before creep loading increases the steady-state creep rate and creep ductility and may or may not increase the time to rupture.
- Short-term aging increases the fatigue life and creep-fatigue life of type 316 stainless steel by strengthening the grain boundaries.
- Long-term aging or service exposure at elevated temperature decreases the room-temperature Charpy impact strength of type 316 stainless steel and its weldments with type 16-8-2 filler metal.

- Aging or dimensionally stabilizing heat treatments can produce very large reductions in the room-temperature Charpy impact strength of CF8M cast stainless steel with initial ferrite contents greater than 15%.

The information obtained to date indicates that the mechanical properties of the austenitic stainless steels types 304 and 316 are satisfactory for the temperature and load conditions anticipated for the design lifetimes of LMFBR out-of-core structures and components.

ACKNOLWEDGMENTS

The authors wish to express their appreciation to R. W. Swindeman and M. L. Grossbeck for reviewing, to Sigfred Peterson for editing and D. L. LeComte for preparation of the manuscript, and to Donna Amburn for preparing many of the figures.

REFERENCES

1. B. Weiss and R. Stickler, "Phase Instabilities During High Temperature Exposure of 316 Austenitic Stainless Steel," *Metall. Trans.* 3, 851–66 (April 1972).

2. "World's Nuclear Reactors, No. 65 — Clinch River," *Nucl. Eng. Int.* 19, 843 (October 1974).

3. C. R. Brinkman, V. K. Sikka, and R. T. King, "Mechanical Properties of Liquid-Metal Fast Breeder Reactor Primary Piping Materials," *Nucl. Technol.* 33, 76–97 (1977).

4. V. K. Sikka, C. R. Brinkman, and H. E. McCoy, Jr., "Effect of Thermal Aging on the Tensile and Creep Properties of Types 304 and 316 Stainless Steels," pp. 316–50 in *Structural Materials for Service at Elevated Temperatures in Nuclear Power Generation*, ed. A. O. Shaffer, MPC-1, The American Society of Mechanical Engineers, New York, 1975.

5. V. K. Sikka, "Elevated Temperature Ductility of Types 304 and 316 Stainless Steel," pp. 129–48 in *Ductility and Toughness Considerations in Elevated Temperature Service*, MPC-8, The American Society of Mechanical Engineers, New York, 1978.

6. V. K. Sikka and C. R. Brinkman, "Influence of Prior Creep Strain on the Short-Term Properties of Types 304 and 316 Stainless Steel," pp. 497–501 in *Proc. 2d Int. Conf. Mechanical Behavior of Materials*, American Society for Metals, Metals Park, Ohio, 1976.

7. R. W. Swindeman, V. K. Sikka, and R. L. Klueh, "Residual and Trace Element Effects on the High-Temperature Creep Strength of Austenitic Stainless Steels," *Metall. Trans. A* 14A, 581–93 (April 1983).

8. V. A. Biss and V. K. Sikka, *Metallographic Study of Type 304 Stainless Steel Long-Term Creep-Rupture Specimen*, ORNL/TM-7618, Oak Ridge National Laboratory, Oak Ridge, Tenn., January 1981.

9. C. F. Etinne, W. Dortland, and H. B. Zeedijk, "On the Capability of Austenitic Steel to Withstand Cyclic Deformation During Service at Elevated Temperature," pp. 225.1–9 in *Int. Conf. Creep Fatigue in Elevated Temperature Applications*, vol. 1, the Institution of Mechanical Engineers, London, 1975.

10. F. G. Wilson, "The Morphology of Grain and Twin Boundary Carbides in Austenitic Stainless Steels," *J. Iron Steel Inst. (London)* **209**, 126–30 (1971).

11. D. P. Edmonds, R. T. King, and G. M. Goodwin, "Residual Elements Have Significant Effects on the Elevated-Temperature Properties of Austenitic Stainless Steel Welds," pp. 56–68 in *Properties of Austenitic Stainless Steels and Their Weld Metals (Influence of Slight Chemistry Variations)*, ASTM STP 679 American Society for Testing and Materials, Philadelphia, 1979.

12. D. P. Edmonds, D. M. Vandergriff, and R. J. Gray, "Effect of Delta Ferrite Content on the Mechanical Properties of E308-16 Stainless Steel Weld Metal. III. Supplemental Studies," pp. 47–61 in *Properties of Steel Weldments for Elevated Temperature Pressure Containment Applications*, ed. G. V. Smith, MPC-9, American Society of Mechanical Engineers, New York, 1978.

13. R. T. King, J. O. Stiegler, and G. M. Goodwin, "Relation Between Mechanical Properties and Microstructure in CRE Type 308 Weldments," *Weld. J. (Miami)* 53, 307–13-S (1974).

14. E. I. Landerman and W. H. Bamford, "Fracture Toughness and Fatigue Characteristics of Centrifigally Cast Type 316 Stainless Steel Pipe After Simulated Thermal Service Conditions," pp. 99–128 in *Ductility and Toughness Considerations in Elevated Temperature Service*, MPC-8, American Society of Mechanical Engineers, New York, December 1978.

15. M. P. Malone, "Sigma and 885°F Embrittlement of Chromium-Nickel Stainless Steel Weld Metals," *Weld. J. (N.Y.)* **46**, 241–53-s (1967).

16. A. Trautwein and W. Gysel, "Influence of Long-Time Aging of CF8 and CF8M Cast Steel at Temperatures Between 300 and 500°C on Impact Toughness and Structural Properties," pp. 165–89 in *Stainless Steel Castings*, ed. V. G. Behal and A. S. Melilli, ASTM STP 756, American Society of Testing and Materials, Philadelphia, 1982.